Delivery of *Exogenous* Imaging Probes for Cellular Microscopy

BY

SHABNAM MOHANDESSI

B.S., University of Shahid Beheshti (SBU), Tehran, Iran, 2003

M.Sc., Chemistry& Chemical Research Center of Iran (CCERCI), Tehran, 2006

THESIS

Submitted as partial fulfillment of the requirements for
the degree of Doctor of Philosophy in Chemistry
in the GRADUATE COLLEGE of
the University of Illinois at Chicago (UIC), 2013

Chicago, Illinois

Defense Committee:

Lawrence W. Miller, Chair and Advisor

Brian Kay, Biological Sciences

Wonhwa Cho, Chemistry

Preston T. Snee, Chemistry

Jung-Hyun Min, Chemistry

This thesis is dedicated to
my lovely Mom, Mahin and my sister, Sherry for their unconditional love,
teaching me not to give up, being strong, and believing in myself
and
to my brothers, Shahab and Shahin for their smile and encourages,
and
to the memory of my beloved Dad, who motivated me and wished to see me as a scientist,
and
last but not least to my lovely fiancé for his endless love and support

ACKNOWLEDGEMENT

"The heavenly spheres which in this domain reside,

Have bewildered the wise,

Thinking far and wide;

Behold and don't lose the trail of wisdom,

For the price of wisdom is to reel to every side"

- Omar Khayyam, Persian polymath and poet

This dissertation would not have been possible without the guidance and the help of many individuals who helped me to start and finish this journey. First of all, I would like to thank my advisor Professor Lawrence W. Miller for his generous support, and kindness during these years. With his guidance, I learned critical thinking and research skills that helped me reached to this point. Also, I would like to thank my dissertation committee members: Dr. Wonhwa Cho, Dr. Jung-Hyun Min, and Dr. Preston T. Snee for everything they taught to me that contributed to my growth as a chemist and researcher, and special thanks to Dr. Brian Kay for his kind support and invaluable advices during this process.

Five years ago, I joined the Department of Chemistry with the help of Professor Tim Keiderling, and Ms. Pat Ratajczyk. I would like to declare my sincere gratitude to them who opened up many opportunities for me to start a challenging but remarkable experience of my life. If it was not their support, I did not have a chance to come to UIC and pursue my PhD studies. Moreover, I would

like to especially thank Professor Richard Kassner for his valuable remarks and advices during all these years.

I would like to acknowledge the financial and technical support provided by Dr. Darren Magda from Lumi4 Incorporation during my studies. The people in the Department of Chemistry have been always very friendly providing a great environment for students, and I am grateful for their assistance especially Ms. Silvia Solis, Ms. Rhonda Staudohar, Mr. Randy Puchalski, Ms. Jackie S. Watts and Ms. Jennifer L. Kazin for their kindness, and help in all these years. Graduate school would be sweet with nice lab mates. I would like to thank my nice lab mates especially Engin, Megha, Xiaoyan, Caitlyn, and Ting that made a friendly environment in the lab.

I owe my deepest gratitude to my supportive family. I was not able to make this journey happen without the support of my lovely family, especially my sincere thanks to my mother, Mahin and my sister, Sharareh for their unconditional love, and support that have been my inspiration as I hurdle all the obstacles in these years. They taught me how to fight with challenges and how to believe in myself. I thank my brothers, Shahab who always inspired me with his cheers and Shahin who always encouraged me with his thoughts. Last but by no means not least, I acknowledge my fiancé, Reza, for his support. He was always there for me both on good days and bad days. He walked through this process with me shoulder to shoulder.

SM.

TABLE OF CONTENTS

CHAPTER **PAGE**

TABLE OF CONTENTS (continued)

CHAPTER **PAGE**

TABLE OF CONTENTS (continued)

CHAPTER **PAGE**

TABLE OF CONTENTS (continued)

CHAPTER **PAGE**

TABLE OF CONTENTS (continued)

CHAPTER **PAGE**

LIST OF TABLES

TABLE **PAGE**

LIST OF FIGURES

FIGURES **PAGE**

LIST OF FIGURES

FIGURES **PAGE**

LIST OF FIGURES (continued)

FIGURES **PAGE**

LIST OF ABBREVIATIONS

BirA	*E. coli* biotin ligase
CFP	Cyan fluorescent protein
CPP	Cell-penetrating peptide
DMEM	Dulbecco's modified eagle media
eDHFR	*Eschericia coli* dihydrofolate reductase
EDTA	Ethylenediaminetetraacetic acid
FlAsH	Fluorescein arsenical hairpin binder
FLIM	Fluorescence lifetime imaging microscopy
FRET	Förster resonance energy transfer
GFP	Green fluorescent protein
GAG	Glycosaminoglycans
hAGT	O^6-alkylguanine-DNA alkyltransferase
HBSS	Hank's buffered salt solution
HEPES	4-(2-hydroxyethyl)[1]-1-piperazineethanesulfonic acid
ICCD	Intensified charge-coupled device
LplA	Lipoic acid ligase
LED	Light emitting diode
LRET	Luminescene resonance energy transfer
PBS	Dulbecco's phosphate buffered saline
PTD	Protein transduction domain
ROI	Regions of interest

ReAsH	Resorufin arsenical hairpin binder
SLO	Streptolysin O
TAT	Trans-Activator of transcription
TEG-TMP	TriethyleneglycolaminoTrimethoprim
TGM	Time-gated microscopy
YFP	Yellow fluorescent protein

SUMMARY

Optical imaging is widely used to visualize biochemical localizations, reactions and interactions in real time inside living systems. Fluorescence microscopy offers the best combination of sensitivity, spatial resolution and temporal resolution, especially when used to study cultured, adherent mammalian cells. Continued advancement in biological fluorescent microscopy is highly dependent on the development of imaging probes: molecules whose fluorescence is coupled to a particular feature of analytical interest (e.g., pH, calcium ion concentration, viscosity); or molecules that are selectively targeted to a particular protein or other biomolecule. While genetically encoded fluorescent proteins are the most well- developed and widely used type of probe, their photophysical and chemical properties can only be modified to a limited extent by mutating their primary structure. By contrast, organic fluorophores, luminescent nanoparticles and other non-biological fluorescent species are more easily modified using synthetic chemical methods. Therefore, there has been considerable interest in developing small molecules and nanoparticles for live-cell imaging applications.

One key challenge in the development and use of so-called *exogenous* probes for cellular imaging is controlled delivery into the cytoplasm or other sub-cellular location of interest. Nanoparticles, luminescent metal-organic complexes and many organic fluorophores are impermeant to cell membranes, and their use as probes is therefore difficult or impossible.

This dissertation explores a variety of techniques to deliver otherwise impermeant, *exogenous* imaging probes into adherent mammalian cells with the main focus being on the delivery of luminescent terbium complexes that selectively label recombinant fusion proteins. Heterodimers of a macrocyclic terbium complex, Lumi4-Tb, linked to trimethoprim (TMP) bind selectively and with high affinity to *Escherichia coli* Dihidrofolate Reductase (eDHFR). Lumi4-Tb exhibits a long (~ms) luminescence lifetime, and time-gated luminescence microscopy can be used to visualize Tb^{3+} luminescence or Tb^{3+}- to- fluorescent protein, luminescence resonance energy transfer (LRET) signals with a high signal-to-background ratio. With time-gated detection, pulsed illumination excites the specimen, and a delay (~μs) is inserted before detection to eliminate non-specific, short-lifetime (~ns) fluorescence background. Here, time-gated microscopy was used to evaluate delivery of TMP-Lumi4 and other Lumi4 analogs into live cells and specific labeling of eDHFR fusion proteins.

In Chapter 2, a variety of physical and biochemical methods that enable the delivery of cell-impermeable terbium complexes into the cytoplasm of living cells are described, including microinjection, osmotic lysis of pinocytic vesicles, and reversible membrane permeabilization with the bacterial toxin, streptolysin O (SLO). Each of these methods allowed for the delivery of TMP-Lumi4 heterodimers into the cytoplasm of adherent cells, including NIH3T3 fibroblasts and MDCK epithelial cells.

The adaptation and characterization of these delivery methods represented a critical technical advance in our laboratory's goal to develop time-gated imaging with lanthanide probes for live-cell imaging of protein localization and protein-protein interactions. In Chapter 3, the use of argninine-rich cell penetrating peptides (CPPs), including nona-arginine and HIV Transactivator of Transcription (Tat)-derived sequences as delivery vehicles for protein-targeted terbium probes is described. Conjugation of CPPs to Lumi4-Tb and TMP-Lumi4 heterodimers allowed for controlled delivery into the cytoplasm and nucleus of various cell types. Time-gated microscopy of Tb^{3+} luminescence and Tb^{3+} mediated LRET signals showed that CPP conjugates could be made to directly translocate from extracellular medium into the cytoplasm under appropriate experimental conditions, and that the probes specifically labeled eDHFR fusion proteins. The results presented in Chapter 3 are the first example of CPP-mediated applied to intracellular protein labeling with cell-impermeable probes.

In Chapter 4, cytoplasmic delivery of nonaarginine-conjugated, benzyl guanine-Lumi4 and benzyl-cytosine-Lumi4 heterodimers and covalent binding of benzyl-guanine-Lumi4 to its respective substrate (SNAP-Tag) is demonstrated using time-gated microscopy. Additional results showing real-time uptake of TMP-Lumi4-Arg9 into MDCK cells as well as the temperature dependence of uptake mechanism in different cell lines are presented. With these studies, which are ongoing in the Miller laboratory, the goals are to extend CPP-mediated delivery to other protein tagging systems besides TMP/eDHFR, enable delivery of

other types of fluorescent probes, and to quantitatively understand CPP-mediated delivery so as to make it widely available as a tool for live cell microscopy with exogenous probes. Taken together, the results presented in Chapters 3 and 4 suggest that CPP-conjugation offers a generally useful strategy for making chemical protein labeling live up to its full potential, where a variety of high-performance fluorophores or other labels can be selectively targeted to one or more fusion proteins in live cells to enable real-time study of protein function. A perspective on the CPP method's potential use and future directions of study is given at the end of Chapter 4.

Chapter 1

CHEMICAL PROBES FOR LIVE CELL IMAGING

]

1.1. Importance of cellular imaging.

The combination of specific probes and optical microscopy makes it possible to study biochemical localizations, reactions and interactions inside living systems [1]. While traditional research using purified biomolecules has provided most of our knowledge of biochemical structure and reactivity, certain questions can only be answered by using microscopic imaging methods to dynamically monitor changes in biochemical location, activity, or concentration inside living cells or tissues [2]. For example, regulated changes in sub-cellular calcium ion concentration control many processes including muscle contraction and neuronal signaling [3]. Fluorescent indicators that exhibit changes in emission intensity or wavelength revolutionized the study of calcium signaling [4], making it possible to visualize changes in localized calcium concentration with fluorescence microscopy. Similarly, the use of genetically encoded fluorescent proteins like green fluorescent protein (GFP) has enabled non-invasive microscopic imaging of reporter gene expression, protein trafficking, and changes in protein interactions or activity [5, 6].

For a variety of physical and chemical reasons, fluorescence microscopy offers the best combination of sensitivity, spatial resolution, and temporal resolution needed to study biochemistry in living systems – usually in cultured, adherent mammalian cells. Conventional wide-field (epi-fluorescence) or laser scanning confocal microscopy can routinely detect a few hundred fluorescent molecules with sub-micron spatial resolution and a temporal resolution of hundreds of miliseconds [7]. Specialized microscopies can now routinely detect

even single fluorescent molecules, and superresolution microscopies have pushed the spatial resolution limit of optical microscopy to ~10s of nm [8, 9]. Moreover, imaging of fluorescence lifetime offers a highly quantitative means to monitor changes in protein-protein interactions or fluorescent response to the cellular environment [10, 11].

Continued advancement in biological fluorescent microscopy is highly dependent on the development of probes. These probes can be molecules whose fluorescence is coupled to a particular feature of analytical interest (e.g., pH, calcium ion concentration, viscocity); or molecules that are selectively targeted to a protein or other biomolecule to enable, for example, trafficking studies. Though, fluorescent proteins are the most widely used labels for biological imaging, they can only be modified to a limited extent by mutating their primary structure. By contrast, organic fluorophores, luminescent nanoparticles and other non-biological fluorescent species can be much more easily modified using synthetic chemical methods. Therefore, there has been considerable interest in developing small molecules and nanoparticles for live-cell imaging applications [12-15].

One key challenge in the development and use of so-called *exogenous* probes for cellular imaging is controlled delivery into the cytoplasm or other sub-cellular location of interest. Nanoparticles, luminescent metal-organic complexes, and many organic fluorophores are impermeant to cell membranes, and their use as probes is therefore difficult or impossible. This dissertation focuses on methods to deliver otherwise impermeant probes into the cytoplasm of live cells

for microscopic imaging. The remainder of this chapter details chemical and physical aspects that make for useful probes as well as physical and biochemical methods for controlled intracellular delivery of probes.

1.2. In vivo protein labeling using *exogenous* probes for cellular imaging.

Currently, fluorescent proteins are used routinely to investigate the behavior of proteins in live cells. While fluorescent protein fusions are immensely useful, the technology nevertheless has its disadvantages. For example, the chromophore in GFP is located inside the protein's beta-barrel structure, and this structure makes it difficult to engineer GFP to be sensitive to the local chemical environment [6]. Furthur, the addition of a relatively large tag (~27 kDa for GFP) may perturb the target protein's cellular function. Finally, the excitation and emission spectra of fluorescent proteins are broad, and the molecules photobleach more easily than many organic fluorophores or nanoparticles. These features make it challenging to use fluorescent proteins for multi-color or single molecule imaging applications. For all these reasons, new approaches have been developed to chemically tag proteins in living systems with small molecules that can be modified synthetically to have desired photophysical or photochemical properties [12, 16].

1.2.1. Chemical protein labeling methods.

In general, chemical protein labeling strategies rely on selective covalent or non-covalent interaction between genetically encoded "receptor" proteins or

peptides and small molecules that are introduced into the cells. The methods are more properly described as a combination of genetic and chemical approaches. A variety of systems have been introduced, and they are described briefly below.

FIAsH labeling technology is one of the first labeling technologies that was reported by Tsien and co-workers in 1998 [17]. FlAsH binds to a short 15 amino acid polypeptide tag with a tetracysteine core (CCXXCC) that is covalently labeled with a fluorogenic bisarsenical fluorescein ligand whose fluorescence increases upon binding. A red-shifted, resorufin-based analog is also available (ReAsH). Following expression of a tetracysteine tag fusion protein in living cells, a bisarsenical dye is added to cell culture that passively diffuses into cells, and selectively binds the tag with sub-nanomolar affinity when a metal-ligand bonds are formed between the tetrecysteine motif (Cys-Cys-X-X-Cys-Cys) and two arsenics in the dye [18, 19]. This method has been applied to study protein structure [20] and protein aggregation in Alzheimer's and Huntington's disease [21-24]. Nevertheless, the FlAsH technology is limited by nonspecific labeling of thiol-rich biomolecules in the cell and also the toxicity of the bis-arsenical ligands. [19, 23]. Also, the system is not modular, meaning that only fluorophores that contain a xanthene moiety can be made into bis-arsenical analogs that bind the tetracysteine peptide.

SNAP-Tag™ and CLIP- Tag™ technologies were developed by Johnson and co-workers [24-28]. SNAP-Tag™ and CLIP-Tag™ are small (~22 kDa) proteins engineered from O^6-alkylguanine-DNA alkyltransferase (hAGT), a DNA repair protein. It is a self-labeling protein technique in which a protein of interest

is fused to the appropriate hAGT mutant. Labeling occurs through an alkylation reaction between hAGT and a benzyl guanine (SNAP) or benzyl cysosine (CLIP) substrate, yielding a covalently modified protein. Several heterodimers of SNAP/CLIP substrates linked to different fluorophores have been prepared [27, 29]. SNAP-tag has been applied to determine protein localization, dynamics and trafficking in live cells [30-32].

A slightly different protein labeling strategy was developed by the Ting laboratory. Here, an enzyme-mediated reaction between a substrate and a peptide tag fused to a protein of interest gives covalently modified proteins. The *E. coli* biotin ligase (BirA) enzyme, whose natural function is biotinylation of proteins containing a peptide recognition motif, was used to label a 15 amino acid peptide tag with a biotin analogue, that can then be subsequently modified with a fluorophore . Intracellular, BirA-mediated protein labeling is difficult because endogenous biotin outcompetes the modified biotin analog as a substrate [33, 34]. Similar to BirA, the Ting lab optimized lipoic acid ligase (LplA) to accept a fluorescent coumarin as a substrate, allowing intracellular labeling [35].

The interaction between trimethoprim (TMP) and *E. coli* dihydrofolate reductase (eDHFR) was exploited by Miller and Cornish to develop a method for non-covalently labeling fusion proteins in live cells. In this method, the target protein is tagged with *E. coli* dihydrofolate reductase (eDHFR). Because eDHFR binds TMP with high affinity (~1 nM K_D) and selectivity (affinities for mammalian DHFRs are K_D > 1 μM), the eDHFR tag can be labeled stoichiometrically with TMP probe heterodimers that bind with a dissociation

half-life of tens of minutes [12, 15, 16, 36]. Our lab has used this system extensively to develop methods for labeling proteins in live cells with lanthanide probes [37, 38].

1.2.2. Designing protein tags for live cell applications.

There are several features that should be considered when designing chemical protein labels for intracellular imaging applications. The first and most important factor is that the organic fluorophore ligand or substrate must be cell-permeable and have no specific binding to endogenous proteins or other biomolecules. Secondly, the ligand or substrate derivatives should be easily synthesized with minimally disruption to the receptor binding or enzyme function. Third, the protein or peptide receptor should be monomeric with a small size. Fourth, the labeling reaction between the protein tag and the ligand/substrate probe should be rapid and near quantitative [16].

While the above-mentioned systems and others meet some or all of these criteria, every chemical protein labeling technology is fundamentally limited by the cell permeability characteristics of the fluorescent or otherwise functional probe molecule. In other words, many of the most desirable fluorophores for microscopy applications are cell impermeable, which has prevented chemical protein labeling from reaching its full potential.

1.3. Probes for live-cell fluorescence microscopy.

Fluorescence microscopy extracts information (intensity, lifetime, polarization) from the emission of luminescent molecules within the cell. The relative lack of naturally occurring fluorescent molecules, however, requires the use of extrinsic imaging probes, which are either recombinantly expressed or added to the cell in order to derive information about the system. Regardless of the type of microscopy or probe, certain features are desirable: 1) probes should be bright, i.e., be highly absorptive of excitation light and emit with a high efficiency, or quantum yield; 2) probes should emit large numbers of photons before photobleaching; 3) probe spectra should be narrow to allow for the separation of multiple signals in a single specimen. Imaging probes that meet some or all of these criteria may be based on organic fluorophores, quantum dots, recombinant proteins, or emissive metal complexes such as lanthanide complexes (LCs) [39, 40] as described in the next sections.

1.3.1. Organic fluorophores.

The synthetic chemistry of organic fluorescent dyes goes back to the 1800's, when quinine was first isolated and characterized. Since then, thousands of different types of small molecule fluorophores, usually polycyclic aromatic compounds have been prepared. Biological microscopy often uses coumarins, xanthenes (e.g., flurorescein, rhodamine) and cyanine dyes (e.g., Cy3, Cy5). Organic dyes have greater color variation and often have higher brightness and resistance to photobleaching when compared to fluorescent proteins. Moreover,

organic fluorophores can be synthetically modified so that their emission intensity, wavelength, or lifetime can change in response to ion concentration, pH, or other parameters of interest [41].

1.3.2. Quantum dots.

Semiconductor nanocrystals, or quantum dots, offer several features that make them attractive for cellular imaging: 1) they are extremely bright due to their high absorptivity (~10^6 $M^{-1}cm^{-1}$; 2) they have size-depended emission wavelengths and are thus available in many colors; 3) they are extremely resistant to photobleaching which is valuable for single-molecule imaging [42]. To make QDs water soluble and compatible with biological systems, they are often encapsulated in cross-linked, amphiphilic organic compounds; however, and this surface modification increases the particle size to 20-30 nm. Because of their relatively large size, delivery of QDs into live cells presents a significant challenge [13, 14, 43]. The development of smaller QDs that can be easily functionalized and that exhibit low levels of cytotoxicity and non-specific binding to cells is an ongoing area of intense research [44].

1.3.3. Luminescent lanthanide complexes.

Organic complexes of trivalent lanthanide ions, (esp. Tb^{3+}, Eu^{3+}) have unique photophysical properties that could be useful for cellular imaging: 1) multiple, narrow emissions (<10 nm at half-maximum) and large Stokes Shifts (>150 nm) that enable efficient signal separation; 2) long emission lifetimes

(~ms) that enable time-gated detection and resistance to self-quenching so multiple labels can be linked to a single target; and 4) good resistance to photobleaching. With time-gated detection, a short pulse of light is used to illuminate the sample, and a brief delay (~μs) before detection of long-lived lanthanide emission that is free from scattering, autofluorescence, and other non-specific short-lifetime (~ns) background signals. Structurally, lanthanide complexes (LCs) consist of a sensitizer or antenna chromophore that absorbs near-UV (320-400 nm) excitation light, and a chelating moiety that holds the metal ion [45, 46]. It is the cellular delivery and use of lanthanide probes for cellular imaging that is the primary focus of the studies presented in this dissertation.

1.4. Föster Resonance Energy Transfer (FRET).

Föster Resonance Energy Transfer (FRET) is the non-radiative energy transfer from an excited state of a luminescent donor molecule to an acceptor molecule (not necessarily luminescent) that is in close proximity (**Figure 1.1**). This energy transfer occurs only if: 1) the emission spectrum of the donor overlaps with the excitation spectrum of the acceptor; 2) the dipoles of both species (i.e. donor emission dipoles and acceptor absorption dipoles) are appropriately oriented; and 3) both species are sufficiently close to one another (<10 nm). FRET is very sensitive to changes in the relative distances of donor and acceptor with dependence on $1/r^6$. These changes can be observed and quantified to not only measure the distance between the donor and acceptor but

also to monitor relative changes in the interactions of donor- and acceptor-labeled molecules [46-48].

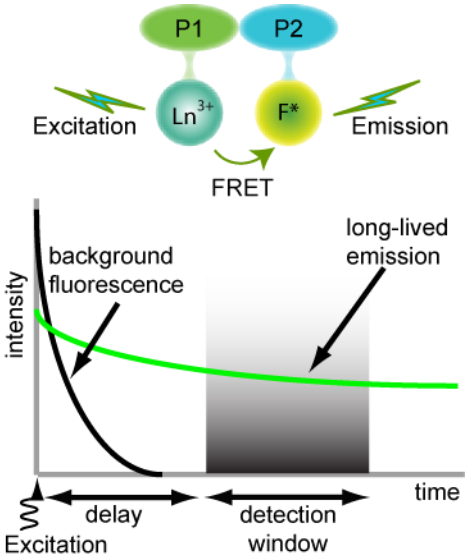

Figure 1.1. Time Resolved Luminescent Resonance Energy Transfer.

1.5. Luminescence Resonance Energy Transfer (LRET).

In a FRET system that comprises a long-lived LC donor and a short-lived (~ns) fluorescence acceptor, the donor-sensitized acceptor emission will exhibit a lifetime equal to the lanthanide donor (~ms). [32, 46, 49, 50]. By using time-gated detection, lanthanide-sensitized acceptor emission is temporally separated from directly excited acceptor fluorescence or other background signals, and the narrow LC donor emission is easily filtered from the acceptor signal. As the emission of lanthanides is not technically fluorescence (singlet- singlet transition), FRET between an LC and a conventional fluorophore is sometimes referred to as luminescence resonance energy transfer, or LRET. LRET-based assays of

molecular interactions, where one species is labeled with a lanthanide complex (usually terbium or europium) and the other with a conventional, short-lifetime fluorophore, are widely used for high-throughput screening because of the inherent sensitivity. Our lab has sought to apply lanthanide probes as donors for imaging protein-protein interactions in living cells.

1.6. Delivery techniques for imaging probes.

One of the critical steps in cellular imaging is the efficient and controlled delivery of probes into the desired sub-cellular location of living cells [51]. The cell membrane acts as a barrier for most imaging probes, including organic fluorophores, quantum dots, and inorganic complexes such as lanthanide complexes. Depending on the size, charge, molecular weight, and polarity, a given probe might be partially permeable or totally impermeable [52]. For instance, fluorescein, rhodamine, Cy5, and Cy3 are all potent fluorescent probes; however, their application in cellular imaging is limited by their low cellular permeability [53]. Therefore, there is a high demand for an efficient delivery method to deliver the imaging probes into the living cells. Potentials of efficient delivery techniques are defined based on probe uptake efficiency, controlling probe delivery, cellular damage, and ease of use of the technique as well as its reproducibility in various cell lines. Substantial progress has been made in the design of new technologies to improve cellular uptake of therapeutic compounds [54, 55]. In the next section, some of these techniques including microinjection,

osmotic lysis of pinosomes, streptolysin *O* (SLO), and cell-penetrating peptides (CPPs) are described [56].

1.6.1. Microinjection.

Microinjection is one of the methods to insert fluorescent probes, protein labels, and antibodies into living cells. This technique has some advantages and limitations. It is an economical method in terms of the amount of the probe that is injected into the living cells which is in the order of a femtoliter; and also, most of delivery methods need at least few microliters of the fluorophore. Microneedle microiniection requires extremely small amounts of starting material and allows precise targeting of the microinjection both temporally and spatially. In addition, it is possible to accurately inject the same cells more than once [57].

In terms of limitations, this technique needs specialized skill and expensive equipment compared with other methods. Also, an obvious limitation of this approach is the low number of cells that can be injected at any given time. Furthermore , microinjection can often be damaging to the cell and can interfere with normal cell function. This has led to a number of alternative methods that could be more efficient and less invasive than microinjection [51, 58].

1.6.2. Reversible membrane permeabilization of the cells using Streptolysin O (SLO).

One non-endocytic delivery method is based on the use of pore-forming toxins. Streptolysin O (SLO) is a pore-forming endotoxin that binds to cell

membranes that has been used as a simple and rapid method to deliver oligonucleotides into eukaryotic cells. SLO binds as a monomer to cholesterol and oligomerizes into a ring-shaped structure to form pores of approximately 25–30 nm in diameter, allowing the influx of both ions and macromolecules. In fact, SLO allows for the delivery of molecules with up to 100 kDa molecular weight to the cytosol [59, 60]. This can be achieved by introducing the mixture of fluorophores with SLO to the living cells. Since cholesterol composition varies with cell types, the permeabilization protocol needs to be optimized for each cell type by varying temperature, incubation time, cell number, and SLO concentration, and activity. Therefore, it is very difficult to obtain a consistent method for various cell lines without compromising the cell membrane. All these limitations make this method the least favorable delivery methods for us.

1.6.3. Osmotic lysis of pinocytic vesicles.

One of the the endocytic pathways is based on cell permeabilization using osmotic lysis of pinocytic vesicles. In this technique, cells are first incubated in culture hypertonic medium containing a high concentration of glucose and fluorophore to be transferred into the living cells. In this step, most pinocytic vesicles are formed by surrounding the fluorophores and trapping them into vesicles which are internalized into the cells through pinocytosis mechanism. Cells are then placed in hypotonic medium containing low concentration of glucose. In the presence of low concentration of sucrose, the pinocytic vesicles burst and, thereby release the fluorophores. This method can be used to deliver

macromolecules up to 70 kDa into the cytosol of living cells One of the limitations of this method is that it is impossible to control the amount of fluorophores delivered into the cells. Another limitation is its difficulty to optimize this technique for any cell line and that compromise the cell membrane as well [61]. These disadvantages may cause significant perturbations to the cell metabolism.

1.6.4. Cell-penetrating peptide (CPPs).

Cell-penetrating peptides (CPPs) are usually short polycationic peptides of less than 20 amino acids enriched in basic residues that are able to penetrate into the cell membrane carrying large variety of cargos including plasmid DNAs, oligonucleotides, small interfering RNAs, proteins, contrast agents, drugs and nanoparticles through the cell membrane [52, 62-64].

The history of Cell-penetrating peptides goes back to 1988 when Frankel and Pablo discovered that the human immunodeficiency virus (HIV) encodes several regulatory proteins that are not found in other retroviruses. They observed that the transcription transactivating (Tat) protein of HIV-1 protein which is 86 amino acids long and contains a highly basic region (with two lysine and six arginines) internalized and localized in the cell nucleus *in vitro* [65, 66]. Later on, other researchers including Prochiantz reported that *Drosophila* Antennapedia homeodomain could be internalized by neuronal cells in 1991 [67] and these findings led to the discovery of the first CPP or PTD termed penetratin in 1994 [62]. The first report of *in vivo* application of CPPs was demonstrated by the

groups of Dowdy for the delivery of small peptides and large proteins [68-70]. After all these progresses, many other CPPs were designed that triggered the movement of a cargo across the cell membrane into the cytoplasm [71-74]**.**

1.6.4.1. CPP Composition and importance of arginine in their translocation efficiency.

There are several reports on CPP categories and composition. Most of them divide CPPs into subgroups defined by their origin or sequence characteristics. For instance, Tat and penetratin peptides are protein- driven peptides and they are called protein transduction domains (PTDs). Polyarginine peptides are also artificially synthesized [75]**.** Among all these peptides, Tat-(48–60), and nonaarginine have been mostly studied by many researchers.

CPPs are not cell specific and they translocate in most of the cells but there have certain features that are crucial for their translocation activity, including the number of basic amino acids especially arginine, charge, and type as well as order of amino acids. It has been reported that presence of basic residues of arginine and lysine has a critical role in their translocation efficiency and cellular localization [75-80]. Whereas arginine and lysine are both positively charged amino acids, further studies have demonstrated that cell-penetrating peptide with higher number of arginine residues are significantly more effective in cellular uptake than lysine polypeptides [76, 81].

Specifically, Wender and Futaki demonstrated that polyarginine sequences (Arg_n) have a substantial role in delivery of biomolecules into living cells, they proposed

that the uptake mechanism involves a bidentate hydrogen-bonding interaction between a guanidinium group of arginine residues and a phosphate group in the membrane [64, 75, 81, 82]. In consistent with previous reports, some other researchers proposed that both lysine and arginine interact with phosphate groups at low temperature, whereas the lysine-phosphate interaction is much weaker than the arginine-phosphate interaction at high temperatures and therefore guanidinium side chain of arginine forms a stronger ion pair with lipid head groups of cell membrane [83]**.** Moreover, in arginine-rich peptides, one of the key factors estimating the transduction efficiency of a CPP is the number and order of amino acids [75, 76, 84].

1.6.4.2. Strategies of CPP linkage to cargos.

As described earlier, CPPs act as vehicles to deliver various cargos, imaging agents, and therapeutic molecules into living cells. Depending to the cargo, these peptides are either covalently or non-covalantly attached to a cargo. For instance, peptides, DNA, and proteins form a complexes with polycationic cell-penetrating peptides while imaging agents such as quantum dots, and organic fluorophores are covalently conjugated to these peptides often through disulfide or peptide bonds. The other cargos such as nanoparticles form a complex with CPPs [85, 86].

1.6.4.3. Proposed mechanisms of cellular uptake of arginine-rich peptides.

There has been a decade of research that researchers are investigating the exact mechanism of internalization of these peptides into the live cells and it is still the subject of debate. However, previous reports agree that there are two main energy-dependent and direct penetrations mechanism for their intracellular delivery. The mechanism of internalization of these peptides varies depending to the chemical and physical properties of the transducing peptide sequences, their concentration, the biophysical characteristics of the cargo, the cell type-dependent composition of the plasma membrane, temperature and size of the cargo.

1.6.4.3.1. Energy-dependent pathways: endocytosis.

One of the most frequently proposed mechanisms for the internalization of CPPs is based on endocytosis pathways. Endocytosis is the process by which components situated in or in close proximity to the plasma membrane are internalized into the cell via vesicles of different characters via variety of different mechanisms. Endocytosis pathways have been categorized differently by various researchers. One of these classification is presented by Conner et al. and including clathrin-mediated endocytosis, caveolae-mediated endocytosis, macropinocytosis, and clathrin- and caveolae-independent endocytosis, all of which are examples of pinocytosis [87].

Macropinocytosis is associated with the inward folding of the outer surface of the plasma membrane, which results in the formation of vesicles called macropinosomes. The resulting macropinosomes are surrounded by a membrane

that is similar to the cell membrane. In receptor-mediated endocytosis, clathrin or caveolin pits are required for cargo uptake. Both clathrin and caveolin proteins are required for invagination of the membrane into the cell cytosol and help to form the vesicles after binding the extracellular molecule to the membrane receptor. Clathrin-coated vesicles are about a 100 nm in diameter, wheras caveolin-coated are about 50–80 nm in diameter [88].

In general, if the CPP conjugated to the fluorophore undergoes to the endocytosis pathway, it is encapsulated within a liposome that usually ends up localized in a lysosome. Liposomes are generally internalized by endocytosis into a vesicle that later fuses with an endosome. Lysosomes are the downstream compartments in this endocytotic pathway, and it is therefore likely that the compound remains in the lysosome. After internalization of the CPP conjugate into the cells, molecules are either degraded or recycled back to the cell surface. However, some peptides go through alternative pathways and translocate into other organelles or into the cytosol [89, 90]. Overall, it has been determined that CPP conjugates especially larger peptide conjugates that internalize into the cells through endocytosis pathways use combination of different pathways in their cellular uptake [91].

1.6.4.3.2. Direct translocation pathways.

Another cellular uptake mechanism that has been reported in the literature is based on direct translocation that depends on many factors, mainly peptide conjugate concentration, temperature, and peptide chemical structure [52, 75, 79,

80, 84, 85, 91]. Further studies on the translocation mechanisms of cell-penetrating peptides (CPPs) at lower temperatures exclude endocytosis pathways as the main translocation mechanism and suggest that some other alternative energy-independent mechanisms are responsible for cellular uptake except endocytosis. As such, several models were proposed to support direct translocation of these peptides into the living cells. Among these models are carpet structure, barrel stave, and inverted micelle models as proposed by Derossi *et al.* [62]. All these models are based on interaction of peptide conjugate with phospholipids and other membrane components that results in destabilizing cell membrane. Carpet structures and barrel staves result in the formation of pores upon interaction of cell-penetrating peptides with cell membrane. However, the inverted micelle model is based upon the interaction of peptide conjugate with cell surface in which a peptide conjugate is trapped in a micelle and its interaction with cell membrane components leads to destabilization of the inverted micelles and consequent release of the peptides into the intracellular milieu.

Duchardt *et al.* showed that, above a critical peptide concentration threshold, internalization occurs through a highly efficient non-endocytic pathway originating from "nucleation zones", spatially restricted membrane regions, leading to a rapid cytoplasmic distribution of the peptide [91]. They further showed that at concentrations below this threshold, penetratin, TAT, and nonaarginine (Arg_9) internalize through a combination of macro-pinocytosis, clathrin-mediated endocytosis, and caveolae-mediated endocytosis depending on the availability of the different pathways [80, 92-95]**.**

Previous research has shown that reduction of extracellular heparan sulfate is related to the peptide uptake [96]. The heparan sulfate molecules are a type of glycosaminoglycans (GAG) on the surface of the cell that are negatively charged and contain sulfate groups to which the arginine residues in arginine- rich peptides bind in a similar way as the binding to the lipid phosphate groups over the surface of lipid bilayer. Some researchers reported that interactions of cationic CPPs with negatively charged glycosaminoglycans (GAG) on the cell surface greatly enhance the endocytic uptake of conjugated macromolecules. Based on these reports, proteoglycans are indirectly effective in peptide conjugate intracellular uptake by distorting membrane fluidity, thereby promoting cell entry of Arg_8, penetratin and Tat via endocytosis pathways [96, 97]**.**

Chapter 2

OPTIMIZATION OF VARIOUS METHODS TO DELIEVR LANTHANIDE COMPLEXES INTO LIVE CELLS.

2. Introduction.

The main objective of the experiments described in this section was to achieve the reproducible delivery of a luminescent terbium complex, Lumi4-Tb, and its derivatives into the cytoplasm of living cells. Specifically, we sought to use time-gated imaging to detect interactions between terbium-labeled proteins and GFP fusions by time-gated imaging of LRET. Selective labeling of eDHFR fusion proteins with TMP-Lumi4 heterodimers was anticipated following cytoplasmic probe delivery. However, we observed that conjugates of TMP to a variety of terbium complexes, including Lumi4-Tb and polyaminnocarboxylates did not enter cells even when cells were incubated in a culture medium containing high concentrations (100 μM) of the conjugates for up to 24 h.[38]. This observation was consistent with published reports indicating that lanthanide complexes are generally membrane-impermeant, and if they enter cells at all, it is usually through an endocytic mechanism [98]. Therefore, to advance cell-based imaging using lanthanide probes, we explored a variety of known methods for achieving cytoplasmic delivery of membrane-impermeant molecules including microinjection, reversible membrane permeabilization, and controlled pinocytosis followed by osmotic lysis of pinocytic vesicles.

Several methods have been used to deliver cell-impermeable molecules such as proteins, nucleic acids, or quantum dots into living cells. These techniques either breach or bypass the plasma membrane to allow passage of the desired cargo into the cytoplasm from extracellular medium, and they can be categorized as physical methods such as microinjection [99], scrape loading, or

bead loading, [100] or as biochemical methods including digitonin-based membrane permeabilization, [60] and the osmotic lysis of pinocytic vesicles [61]. Microinjection has been successfully used for lanthanide complex delivery [49], and the method allows for precise delivery of small (pL) volumes of probe solution into cells with a high degree of spatial and temporal resolution. However, the technique requires specialized apparatus and can only be used to load relatively few cells at a time.

Two biochemical methods were found to be successful for simultaneously loading TMP-Lumi4 luminescent compound into many cells at once: reversible membrane permeabilization with the bacterial toxin streptolysin O (SLO) and osmotic lysis of pinocytic vessicles. Time-gated microscopy of terbium luminescence showed that both methods allowed for cytoplasmic delivery of TMP-Lumi4 into the cytoplasm of live MDCK and NIH3T3 cells, and that TMP-Lumi4 diffused freely throughout the cytoplasm and nucleus. The optimization of SLO-mediated and pinocytic delivery methods was a critical advance that allowed our lab to demonstrate LRET-based imaging of protein-protein interactions using terbium probes [37]. Experimental protocols and results detailing the optimization of SLO-mediated and pinocytic delivery methods are given below, followed by a section describing experimental protocols for adherent cell microinjection.

2.1. Experimental Methods – SLO-mediated and pinocytic delivery of membrane- impermeant probes into adherent cells.

2.1.1. Cell culture.

Hela and MDCKII cells were cultured in Dulbecco's Modified Eagle Media (DMEM, Invitrogen) supplemented with 10% FBS, 2 mM L-glutamine, 100 unit⁄mL penicillin and 100 mg⁄mL of streptomycin at 37 °C and 5% CO_2. Hela and MDCK cells were passaged using 0.05% trypsin/ 0.03% EDTA solution (GIBCO) and 0.25% trypsin/0.03% EDTA solution, respectively.

2.1.2. Luminescent probes.

A stock solution of fluorescein isothiocyanate-dextran (average molecular weight, ~10 kDa; Sigma-Aldrich, Inc.) was prepared by dilution into PBS (conc. = 2 mM). TMP-Lumi4 (300 μM in H_2O) was combined with ~1.2 equivalents of $TbCl_3$, vortexed for 5 min., and allowed to stand at room temperature for 30 min. This step results in the chelation of terbium, rendering the probe luminescent.

2.1.3. Probe delivery via SLO-mediated membrane permeabilization.

SLO (1 mg⁄mL in PBS/50% glycerol, MBL International, Inc.) was diluted to a final concentration of 1000 ng⁄mL in 10 mM DTT/PBS and incubated at 37 °C for 2 h. This step ensures reduction of disulfide bonds and is necessary for SLO activity. The preactivated SLO was aliquoted and stored at −20 °C for later use. In a typical experiment, terbium-chelated TMP-Lumi4 was diluted to 15 μM in 100 μL Hank's buffered salt solution (HBSS). Preactivated SLO was added to a

final concentration of 50 ng⁄mL (1:20 dilution of preactivated SLO stock solution). NIH3T3 or MDCKII cells in a single well of an 8-well chambered slide were washed 3X with prewarmed (37 °C) HBSS. Then, 150 μL of prewarmed probe/SLO/HBSS solution was added, and the cells were incubated at 37 °C and 5% CO_2 for exactly 10 min. After incubation, 300 μL of DMEM containing 1.8 mM Ca^{2+} was added to the cells to effect resealing of membranes. The cells were incubated for at least 1 h at 37 °C and 5% CO_2 before washing 3X w/PBS and immersion in DMEM prior to imaging.

2.1.4. Probe delivery via osmotic lysis of pinosomes.

A 6 μL aliquot of TMP-Lumi4 (300 μM in H_2O) was combined with ~1.2 equivalents of $TbCl_3$ (in ~3 μL H_2O), vortexed for 5 min., and allowed to stand at room temperature for 30 min. The metal-labeled TMP-Lumi4 solution (~9 μL) was combined with 27 μL of hypertonic growth medium (Influx™ reagent, Invitrogen, prepared according to manufacturer's instruction). Importantly, the final solution should be at least 70% hypertonic growth medium to ensure efficient pinocytosis. For fluorescein-dextran, final conc. in hypertonic medium ranged from 50 μM to 200 μM. NIH3T3 or MDCKII cells in a single well of an 8-well chambered slide were washed 1X with prewarmed (37º C) PBS and 2X with prewarmed hypertonic solution, respectively. Then, prewarmed hypertonic solution containing TMP-Lumi4 was added, and the cells were incubated at 37 °C and 5% CO_2 for *exactly* 10 min. The cells were then quickly washed 2X with hypotonic solution (Influx™ reagent, Invitrogen, prepared according to

manufacturer's instruction) and allowed to incubate in hypotonic solution for *exactly* 2 min. at room temperature to effect lysis of pinosomes. The cells were then washed 2X with PBS, immersed in complete DMEM and incubated for ~1 h at 37 °C and 5% CO_2 before imaging.

2.1.5. Microscopy.

Imaging of adherent live cells was performed using a previously described, modified epifluorescence microscope (Zeiss Axiovert 200) [101]. All images were acquired using a EC Plan Neofluar, 63X, 1.25 N.A. objective (Carl Zeiss, Inc.). Filter cubes containing the appropriate excitation and emission filters and dichroics allowed for wavelength selection. Bright field and continuous wave fluorescence images were acquired using an Axiocam MRM CCD camera (Carl Zeiss, Inc.). For time-gated luminescence, pulsed excitation light from a UV LED (λ_{em} = 365 nm, illumination intensity = 0.6 W/cm^2 at the sample plane) was synchronized with the intensifier component of an ICCD (Mega-10EX, Stanford Photonics, Inc.) such that a 10 μs delay was inserted between the end of the LED pulse and the intensifier start-time. For each acquisition, the signal from multiple excitation/emission events was accumulated on the ICCD sensor and read out at the end of the camera frame. The source/camera timing parameters were the same for all of the time-gated images and data presented here: excitation pulse width = 1500 μs, pulse period = 3000 μs, delay time = 10 μs, intensifier on-time = 1390 μs.

2.2. Results and Discussion.

2.2.1. Cellular delivery of fluorescein-dextran mediated by osmotic lysis of pinosomes.

When adherent cells are incubated in a hypertonic medium containing sucrose and polyethylene glycol, they undergo macropinocytosis, and extracellular fluid becomes trapped in vesicles, or pinosomes, throughout the cell cytoplasm. By quickly transferring the cells to a hypotonic medium (e.g., a mixture of DMEM and PBS), the change in osmolarity "shocks" the cells, and the vesicles rupture, releasing their contents into the cytoplasm. This method was first introduced for delivering macromolecules into cells 30 years ago, [61] and kits for preparing the necessary reagents are commercially available (Invitrogen, Inc.).

This method was first attempted using fluorescein-conjugated dextran as the impermeant probe by incubation of NIH3T3 cells in hypertonic growth medium containing 200 μM of fluorescein dextran for 10 min., followed by incubation in hypotonic growth medium for 2 min. resulted in successful loading of ~20% of cells, as evidenced by diffuse fluorescein signals in the cytoplasm (**Figure 2.1**). This experiment was successfully repeated using varied concentrations (100 μM, 50 μM) in the hypertonic loading step.

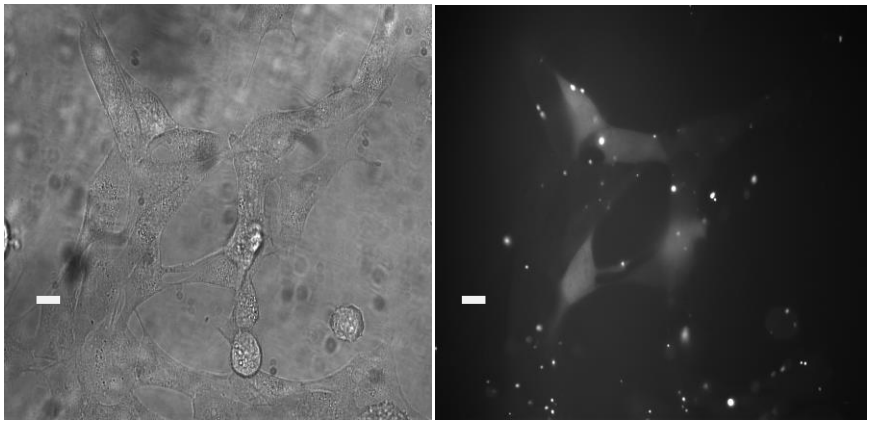

Figure 2.1. Cytoplasmic delivery of fluorescein-dextran via osmotic lysis of pinosomes. NIH3T3 fibroblasts were loaded with 200 μM fluorescein dextran according to protocol described in the text. Micrographs: BF, bright field; CW, continuous wave fluorescence (λ_{ex} = 480 ± 20 nm, λ_{em} = 535 ± 25 nm); scale bars,

2.2.2. Cellular delivery of TMP-Lumi4-Tb mediated by osmotic lysis of pinosomes.

After initial success with fluorescein dextran, the pinocytosis method was used to deliver TMP-Lumi4-Tb into live cells. TMP-Lumi4 (**Figure 2.2a**) selectively binds to eDHFR with nanomolar affinity, but was previously found to be completely impermeable to cell membranes [38]. A single 10 min. incubation with hypertonic medium containing TMP-Lumi4 (final conc. = 50 μM) was sufficient to allow detection of Tb^{3+} luminescence in the cytoplasm of NIH3T3 cells using time-gated luminescence microscopy (**Figure 2.2b**). Repeated experiments showed that both NIH3T3 fibroblasts and MDCK epithelial cells could be reliably loaded (>50% of total cells) with TMP-Lumi4 using the

pinocytosis delivery technique. Because this method does not permeabilize the cell membrane, it should be minimally perturbative to cellular physiology.

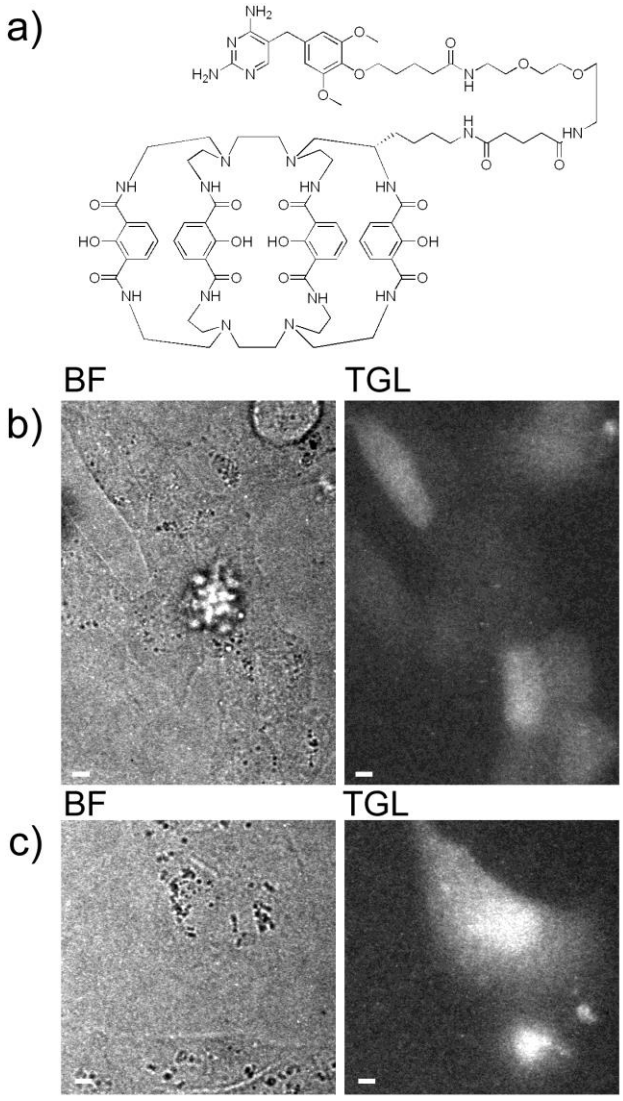

Figure 2.2. Cytoplasmic delivery of TMP-Lumi4 via pinocytosis and SLO-mediated membrane permeabilization. a) Structure of TMP-Lumi4. **b)** NIH3T3 cells loaded with TMP-Lumi4 using pinocytosis. **c)** MDCK cells loaded with TMP-Lumi4 using SLO. Micrographs: BF, brightfield; TGL, time-gated luminescence (λ_{ex} = 365 nm, λ_{em} = >415 nm, delay=10 μs). Scale bars, 10 μm.

Given this feature and the method's reliability, osmotic lysis of pinosomes was initially the lab's most favored technique for delivering lanthanide probes into live cells for imaging experiments.

2.2.3. SLO-mediated delivery of TMP-Lumi4.

In parallel to pinocytosis, the use of SLO for cellular delivery of lanthanide complexes was investigated. SLO is a toxin that oligomerizes to form pores in cell membranes. Importantly, the pore formation process can be reversed by adding Ca^{2+} to cells. Thus, by subjecting cells to a permeabilization step in a medium that contains SLO and probe, followed by a sealing step, molecules that are smaller than the pores (~13 nm) can be imported into the cell cytoplasm. [102]. The challenge here was to identify SLO and probe concentrations that resulted in permeabilization and loading of 60-80% of the total cell population within 15-30 min.

Initial attempts to optimize SLO-mediated delivery using fluorescein dextran were unsuccessful. Although fluorescein dextran (70 kDa) was reported to be amenable to delivery using this technique [59], conditions that yielded consistent delivery into a significant proportion of a cell population could not be identified. However, SLO-mediated delivery was successful for delivering TMP-Lumi4. It was found that 10 min. incubation in HBSS containing 50 ng/ mL SLO and 15 μM TMP-Lumi4 was sufficient to deliver the probe into the cytoplasm of MDCK cells (**Figure 2.2c**). While successful, the fact that SLO permeabilizes cell membranes makes it unattractive for many live cell experiments because

many cellular processes could be negatively affected. Also, the activity of SLO varies from batch-to-batch, and it is fairly tedious to validate its activity and optimize it for use with different cell lines. For these reasons, SLO-mediated delivery has not been used extensively in our lab.

2.3. Microinjection.

Microinjection is the direct-pressure injection of a solution into a cell through a glass capillary. Since its introduction a century ago, [13, 14] microinjection has been optimized to allow precise and reproducible delivery of proteins, nucleic acids or other cell impermeable molecules into live cells with minimal toxicity. The main advantages of microinjection are its precision and high degree of spatial and temporal resolution. Controlled volumes of probe solution can be instantaneously directed to specific sub-cellular regions (e.g., cytoplasm or nucleus). The main disadvantages of microinjection are that it requires a complex apparatus, demands a high degree of skill from the user, and can only be used to load relatively few cells during a given experiment.

In our laboratory, there has not been a critical need yet for microinjection because we have been successful in developing biochemical and peptide-based probe delivery methods. Nevertheless, it is a powerful tool that can be used to evaluate new probes; quantitatively measure the amount of material delivered into a single cell, or potentially be used to deliver probes that may not be amenable to other delivery techniques. Therefore, in this section, I describe the Sutter

Instruments microinjection system available in our lab and provide protocols for its use in live-cell fluorescent probe delivery.

2.3.1. Microinjection System Overview.

2.3.1.1. System Components.

In general, a microinjection system has three main parts: 1) an inverted light microscope to view cells and micropipette during the injection process; 2) a micromanipulator to hold micropipettes or capillaries; and 3) a pressure regulator to direct the outflow of the liquid from the pipette tip. While not part of the injection system itself, a pipette puller is also needed to produce micropipettes of the required dimensions. The system in use in our lab consists of a Sutter Instruments, Inc. XenoWorks™ Micromanipulator and Digital Microinjector mounted on a Zeiss Axiovert 200 inverted microscope (**Figure 2.3**). A P-1000 Micropipette Puller (Sutter Insturments) is used for pipette fabrication.

2.3.1.2. Digital Microinjector.

The Digital Microinjector controls the injection pressure in the capillary needle. A constant compensation pressure is maintained to counterbalance capillary forces and thus maintain the injection solution at the capillary tip. For injection, the pressure is increased to a user-defined injection pressure (application specific) for the duration of the injection. The injection pressure can be applied in pulses of defined duration to control the volume of material delivered.

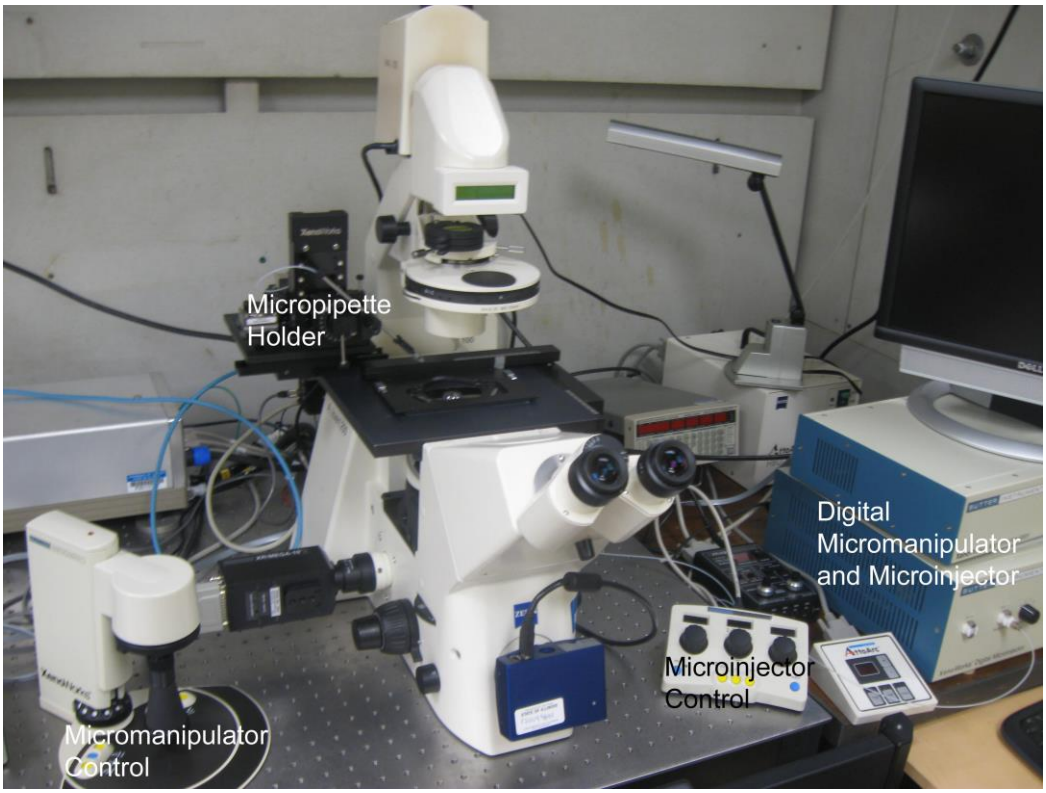

Figure 2.3. Axiovert 200 inverted microscope with Sutter Instruments, Inc. XenoWorks™ microinjection system installed. System components are labeled.

2.3.1.3. Micropipette puller

Micropipettes are fabricated with a micropipette puller. As the name implies, the puller heats capillary tubes while simultaneously pulling them to produce pipettes with tips of controlled length, taper, and end diameter. The tip dimensions are perhaps the most critical parameter for successful microinjection, and they vary depending on the type of experiment they will be used for (e.g., adherent cell microinjection, patch clamp electrophysiology). Pipettes with tips of desired dimensions can be fabricated by using appropriate capillaries and pulling parameters (**Table 2.1**). In this study, thin-walled glass capillary with a borosilicate filament (1 mm O.D. X 0.5 mm I.D. X 10 cm; Sutter Instruments, cat. no. BF100-50-10) were used.

Table 2.1 Effect of Micropipette Puller parameters on pipette tip dimensions.

PARAMETER	INCREASE	DECREASE
Heat	Longer Taper	Shorter Taper, Lower Resistance
Pull	Smaller Tips, Longer Taper	Larger Tips, Shorter Taper
Velocity	Smaller Tips	Larger Tips
Time (ms)	Shorter Taper	Longer Taper
Pressure	Shorter Taper, Lower Resistance	Longer Taper, Higher Resistance

2.3.1.3. Micromanipulator

The micromanipulator makes it possible to control the speed and direction of travel of the micropipette using a joystick. A micropipette holder positions the glass capillary tip required for injection. The micromanipulator includes a joystick that enable user to change the position of the tip either horizontally or vertically in three axes (x, y, z) while focusing the tip to reach to the target cell.

2.3.2. Protocol for Microinjection of Adherent Cells.

2.3.2.1. Materials.

Unless otherwise noted, chemicals were obtained from Sigma-Aldrich, Inc., and cell culture reagents were purchased from Invitrogen, Inc. MDCK cells

were provided by Prof. J.R. Turner, HeLa and NIH3T3 cells were provided by Prof. W. Cho, and HEK293 cells were obtained from the American Type Culture Collection. Lumi4-NH_2 was provided by Lumiphore, Inc.

2.3.2.2. Sample Preparation and Micropipette Filling.

In all experiments, the micropipettes were prepared immediately before use. Before each experiment, solutions containing the probe at a desired concentrations were centrifuged to remove any insoluble debris to avoid tip clogging. Micropipette tips were back-loaded using with at least 1-2 µL of probe solution. In the back-loading method, the tips are inversed into the probe solution and kept at room temperature for less than 1 min. When it is loaded, a bubble will appear at the tip of the capillary glass, indicating successful loading.

2.3.2.3. Cell Culture.

Cells were seeded in 25- or 50-mm tissue-culture plates using the 2 mL growth medium to obtain a low density so that there is minimal contact between adjacent cells. Here, Hela and MDCKII cells were cultured in Dulbecco's Modified Eagle Media (DMEM, Invitrogen) supplemented with 10% FBS, 2 mM L-glutamine, 100 unit⁄mL penicillin, and 100 mg⁄mL of streptomycin at 37 °C and 5% CO_2. Hela and MDCK cells were passaged using 0.05% trypsin/ 0.03% EDTA solution (GIBCO) and 0.25% trypsin/0.03% EDTA solution, respectively.

2.3.2.4. Microinjection Apparatus Set-Up and Injection Technique.

The micromanipulator was first set with all three axes (x, y, z) at the center of their movement ranges. This ensures that one does not run out of travel during an experiment. Then, the Petri dish containing the cell-covered coverslips was located at the center of the microscope stage, and brought into focus in bright field mode using a 63X oil-immersion objective. The loaded micropipette was then placed into the micropipette holder and aligned so that its tip projects into the optical axis of the microscope. At this point, the micropipette tip should not be in contact with any object as it will break very easily. After setting up the micropipette, the cells are focused (**Figure 2.4**) in the microscope field of view

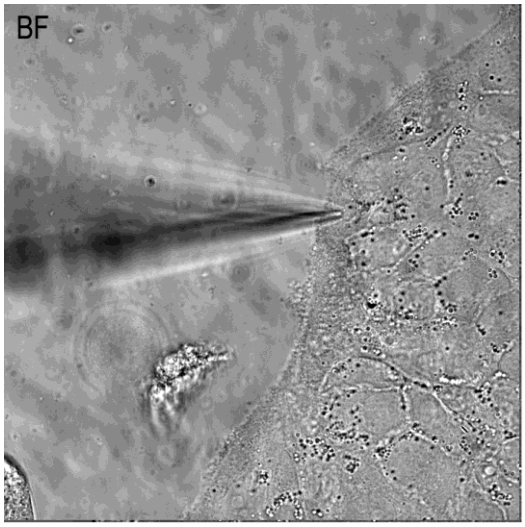

Figure 2.4. Micropipette tip focused on a cytoplasm of MDCK cell exactly before injection on a bright field (BF) view of microscope.

Using the micromanipulator joystick and changing the speed of movement from lowest to highest, the micropipette was centered in the field of view, and then brought into focus. By focusing the microscope up and down, one can view the micropipette tip or the cells. By rotating the Z-axis control of the micromanipulator slowly and very carefully, the micropipette tip is lowered toward the cells. As the cells come into focus, the micropipette tip is stopped, as the tip is now likely located within the cell. The injection is then triggered. For injection into adherent cells, Digital Micoinjector parameters were set as follows: compensation pressure; 40 hPa, injection pressure, 254 hPa; injection pulse duration, 0.2 s.

2.3.3. Results

2.3.3.1. Microinjection of fluorescein dextran.

Fluorescein dextran was injected to both MDCK and Hela cells at different concentrations of 5, 10, 20, and 50 μM with different micropipette tips. The goal was to optimize the pulling program to make a micropipette that could easily inject into any type of cell with lowest concentration and highest signal intensity without damaging the cell membrane. The optimal pulling parameters are shown in **Table 2.2**. As seen in **Figure 2.5**, multiple cells within a field of view could be readily injected with roughly equivalent amounts of probe.

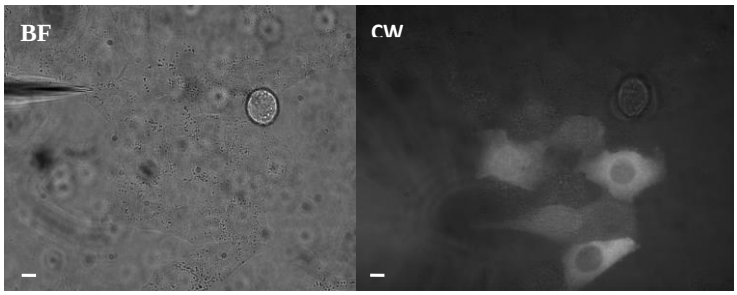

Figure 2.5. Cytoplasmic injection of 10 µM Fluorescein Dextran into Hela cells. Micrographs: BF, bright field; CW, continuous wave fluorescence (λ_{ex} = 480 nm ± 25 nm, λ_{em} = 535 ± 25 nm); scale bars, 10 µm. Multiple cells within a field of view could be successively injected. The micropipette tip is visible in the bright field image.

Table 2.2. Optimized pulling programs.

PULLING PARAMETER	Fluorescein-dextran	Lumi4-Tb-NH2
Heat	**543**	**558**
Pull	**40**	**40**
Velocity	**22**	**18**
Time (cooling time-ms)	**210**	**200**
Pressure (air flow-psi)	**543**	**543**

2.3.3.2. Microinjection of Lumi4-NH_2

After successful optimization of the pulling program for different concentrations of Fluorescein dextran and injection into MDCK cells, the luminescent terbium probe, Lumi4-NH_2-Tb was injected into the cells using the same pulling program. Initially, attempts to inject 10 μM solutions yielded low intensity time-gated luminescence images. Furthermore, it was difficult to obtain consistent results. By increasing the solution concentration to 100 μM, it was possible to obtain brighter luminescent images, and pulling parameters were further optimized (Table 2.2) that allowed for consistent microinjection of Lumi4 into the cytoplasm of MDCK cells (**Figure 2.6**).

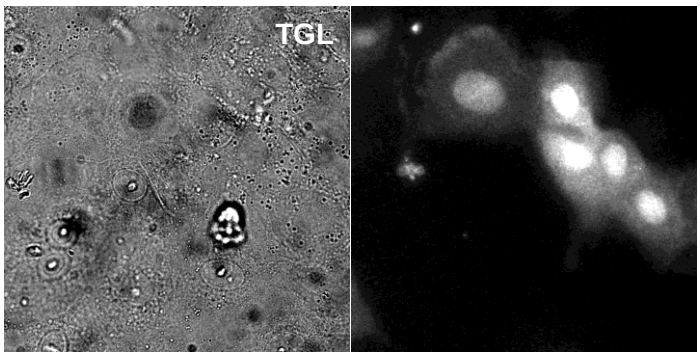

Figure 2.6. Cytoplasmic and nuclear injection of 100 μM Lumi4-Tb-NH_2 into the MDCK cells. Micrographs: on the left, bright field (BF); on the right, time-gated luminescence (TGL) (λ_{ex} = 365 nm, λ_{em} = >415 nm. Multiple cells within a field of view could be successively injected. The micropipette tip is visible in the bright field image.

2.3.4. Microinjection as a quantitative tool.

A potentially useful feature of microinjection is that it makes it possible to know the precise volume of solution, and thus amount of probe, injected. Typically, injection volumes used for adherent cells microinjection are 0.1- 0.7 pL to inject into the cytoplasm and 0.01 to 0.06 picoliters to injection into the nucleus [99]. Our microinjection system was calibrated to determine the exact injection volume. By injecting into a drop of oil on a coverslip, the spherical droplets diameter could be measured by image analysis and its volume calculated as described before [103].

2.3.4.1. Calculation of the volume of injected fluorescent probe using image processing.

Fluorescein dextran (10 μM) was injected into a droplet of oil at the center of a coverslip (**Figure 2.7, bottom**). The diameter of each presumably spherical droplet was measured based on value of pixel in diameter of each droplet using the ImageJ software (3.1 pixel/μm for 63X objective on our system). From a measurement of 14 droplets, a volume of 0.36 ± 0.06 pL was calculated. This volume is within the range considered optimal for cytoplasmic injection into adherent cells (0.1 to 0.7 pL). Assuming that the volume of a cell is approximately 3 pL, [6], injection of 10 μM probe yields a cellular concentration of ~1 μM.

The calculated cellular concentrations (1-10 μM for fluorescein dextran and Lumi4-NH_2) appear to be consistent with the intensity seen in the

fluorescence images of injected cells (**Figures 2.5, 2.6**). Typically, over-expressed fluorescent proteins and small molecule fluorescent indicators are imaged at effective cellular concentrations of 2-20 μM, [6, 104] and the detection limit for visualizing diffuse GFP signals in the cytoplasm with a widefield fluorescence microscope is ~200 nM [105]. Cytoplasmic fluorescence of fluorescein dextran at approximate cellular concentratrion ~1 μM is visualized at high contrast with ~1198.8 ms exposure times and 10-fold higher concentrations of Lumi4-NH_2-Tb are easily detected with only 67 ms exposures. The ability to quantify the amount of probe delivered into cells will be used for measuring intracellular concentration of other impermeant probes.

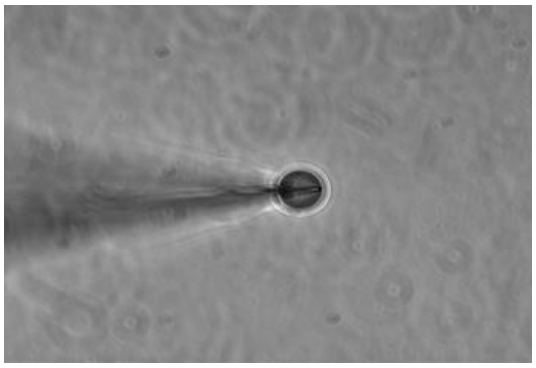

Figure 2.7. Top, Droplet of fluorescein dextran at the tip of micropipette.

2.4. Conclusion.

The techniques presented in this chapter were important for advancing the development of lanthanide probes for cellular microscopy. However, while each technique – SLO-mediated membrane permeabilization, osmotic shock and microinjection – is capable of delivering protein targeted lanthanide probes into the cytoplasm of live adherent cells, they each required careful optimization and are probably not likely to be widely adopted by other laboratories. Therefore, we turned our attention toward developing a more straightforward way to deliver lanthanide complexes or other impermeant probes into the cytoplasm. As detailed in the following two chapters, conjugation to arginine-rich cell penetrating peptides yields lanthanide probes that directly enter the cytoplasm from culture medium, allowing for simple "mix-wash-and-image" experimental protocols.

Chapter 3

CELL-PENETRATING PEPTIDES AS DELIVERY VEHICLES FOR A PROTEIN –TARGETED TERBIUM COMPLEX

3. Introduction.

Chemical protein labeling strategies leverage orthogonal interactions between small molecule ligands and genetically encoded amino acid sequences to attach fluorophores or other useful functionalities to proteins in live cells [12, 15, 36, 106]. Ideally, such approaches could be used to label intracellular proteins with particularly bright and photostable fluorophores (e.g., AlexaFluors, cyanines), [107] photosensitive dyes that facilitate superresolution imaging, [25, 28, 108] or luminescent lanthanide complexes that enable highly sensitive, time-gated microscopy [32, 109]. In practice, however, these types of labels are often impermeable to cell membranes, and chemical labeling approaches have either been limited to studies of cell-surface proteins or have required more onerous methods of intracellular delivery like microinjection or electroporation [25, 28, 32, 108, 109]. For example, our laboratory has recently developed a series of trimethoprim (TMP)-lanthanide complex conjugates that selectively and tightly (~nM K_D) bind to *Escherichia coli* dihydrofolate reductase (eDHFR) [37, 38, 110].With these compounds, the useful properties of lanthanide luminescence (narrow, multi-wavelength emission, long luminescent lifetime) can be easily imparted to recombinant fusion proteins. By selectively labeling eDHFR fusion proteins in live cells with one conjugate, TMP-Lumi4(Tb), we showed that interactions between eDHFR fusions and green fluorescent protein (GFP) fusions could be imaged at high signal-to-background ratio using time-gated, luminescence resonance energy transfer (LRET) microscopy [37].However, intracellular delivery of cell-impermeable TMP-Lumi4-Tb required either

reversible plasma membrane permeabilization or osmotic lysis of pinocytic vesicles, as described in Chapter 2.

In this chapter, we show that covalent coupling to cell penetrating peptides (CPPs) including nonaarginine (Arg9) and HIV Tat-derived sequences (Tat) mediates passive, cytoplasmic delivery of Lumi4(Tb) and TMP-Lumi4(Tb) heterodimers in various cell types. Time-gated microscopic detection of Tb^{3+} luminescence or LRET between Tb^{3+} and a red fluorescent protein revealed that the CPP conjugates directly translocated from culture medium to the cytoplasm, diffused freely throughout the cytoplasm and nucleus, and that TMP-Lumi4(Tb) specifically labeled eDHFR fusion proteins in the nucleus of Maden Darby canine kidney (MDCKII) epithelial cells following CPP-mediated delivery. We also provide direct microscopic evidence of intracellular delivery and reductive cleavage of a disulfide bond between a CPP and its cargo.

3.1. Experimental Methods.

3.1.1. Materials and analyses.

Unless otherwise noted, chemicals were obtained from Sigma-Aldrich, Inc., peptides were obtained from AnaSpec, Inc., and cell culture reagents were purchased from Invitrogen, Inc. H2B-eDHFR was provided by Prof. V.W. Cornish, and pcDNA3-TagRFP-T was obtained from Prof. R.Y. Tsien. MDCK cells were provided by Prof. J.R. Turner, HeLa and NIH3T3 cells were provided by Prof. W. Cho, and HEK293 cells were obtained from the American Type Culture Collection.

UV absorption measurements were recorded on a Varian Cary 300 double beam spectrometer using quartz cells of 1 cm path length. Emission spectra of **1**, **3**, and **4** were measured using a HORIBA Jobin Yvon Fluorolog-3 spectrofluorometer equipped with an IBH TBX-04-D detector. Emission spectra of **2**, **11**, and **17** were measured using a HORIBA Jobin Yvon Fluoromax-3 spectrofluorometer.

3.1.2. Synthesis of peptide conjugates.

The peptide conjugates used in this study were prepared by Darren Magda of Lumiphore, Inc. (Richmond, CA). Complete details of conjugate synthesis and characterization (NMR, MS) have been reported [111].

3.1.3. Metallation with terbium and conjugate luminescence characterization.

Lyophilized conjugates were dissolved in sterile water (conc. = 1 mM) in 1.5 mL microfuge tubes. $TbCl_3$ (~1.2 equiv.) in water was added, and the samples were vortexed ~5 min. and allowed to rest at RT for ~30 min. All samples exhibited bright green luminescence following dissolution in water and addition of terbium when exposed to light from a hand-held UV lamp.

3.1.4. Plasmid preparation.

A mammalian expression vector encoding H2B-TagRFPT-eDHFR was prepared by Megha Rajendran. The gene encoding TagRFP-T was subcloned

from plasmid TagRFP-T pcDNA3 [112] to pRSETb-EGFP-eDHFR [38] to generate pRSETb-TagRFPT-eDHFR. A *BamHI* to *Acc65I* fragment encoding TagRFP-T was prepared by PCR from TagRFP-T pcDNA3 using the primers 5'-GCA TAC GTC GGA TCC GAT GGT GTC TAA GGG CGA -3' (*BamHI*, coding strand) and 5'-GCA TAC GTC GGT ACC CCT TGT ACA GCT CGT CCA T-3' (*Acc65I*, non-coding strand). This fragment was inserted between the *BamHI* site and the *BsrGI* site in pRSETb-GFP-eDHFR to give to pRSETb-TagRFPT-eDHFR. The gene encoding TagRFPT-eDHFR was subcloned from plasmid pRSETb-TagRFPT-eDHFR to H_2B-eDHFR to generate H_2B-TagRFPT-eDHFR. A *BamHI* to *NotI* fragment encoding TagRFPT-eDHFR was prepared by PCR from pRSETb-TagRFPT-eDHFR using the primers 5'- T CGT GAT CTG GAT CCC GCT TCT GCT TCG TCT TCG ATG GTG TCT AAG GGC -3' (*BamHI*, coding strand) and 5'- GCT TTG TTA GCG GCC GCA CCA TGC TTA GAA TCC TTA-3' (*NotI*, non-coding strand). This fragment was inserted between the *BamHI* site and the *NotI* site in H_2B-eDHFR to give to H_2B-TagRFPT-eDHFR. Plasmid integrity was confirmed by direct sequencing.

3.1.5. Cell culture, transfection and labeling.

MDCK, NIH3T3, HEK293, and HeLa cells were cultured in DMEM (+) (Dulbecco's Modified Eagle Media supplemented with 10% FBS, 2 mM L-glutamine, 100 unit⁄ mL penicillin and 100 µg⁄mL of streptomycin) at 37 °C and 5% CO_2. MDCK cells were seeded at 10^5 cells per well into a 6-well plate. After ~18 h incubation at 37 °C and 5% CO_2, adherent cells (~80% confluent) were

transfected with 2 μg of the pH2B-TagRFPT-eDHFR using Lipofectamine2000™ (Invitrogen) according to manufacturer's instructions. Approximately 6 h after transfection, cells were trypsinized and reseeded at 15,000 cells/well into 8-well chambered coverglasses (Nunc™, 12-565-470) and incubated at 37 °C and 5% CO_2 overnight.

Cells growing in DMEM (+) in 8-well chambered coverglasses were washed 1X with PBS and re-immersed in culture medium (with or without FBS) at the desired temperature (37 °C or 4 °C) containing peptides at the desired concentration. Cells were then incubated at 37 °C and 5% CO_2 (on ice in ambient atmosphere for 4 °C studies), washed 2X in PBS, and reimmersed in DMEM (+) supplemented with 1 mM Patent Blue™ dye to quench extracellular luminescence. Following incubation and washing, cells were maintained at 37 °C and 5% CO_2 until imaging.

3.1.6. Microscopy, image processing, and analysis.

Imaging of adherent live cells was performed using a previously described, modified epifluorescence microscope (Zeiss Axiovert 200) [101] . All images were acquired using a EC Plan Neofluar, 63X, 1.25 N.A. objective (Carl Zeiss, Inc.). Filter cubes containing the appropriate excitation and emission filters and dichroics allowed for wavelength selection. Bright field and continuous wave fluorescence images were acquired using an Axiocam MRM CCD camera (Carl Zeiss, Inc.). For time-gated luminescence, pulsed excitation light from a UV LED (λ_{em} = 365 nm, illumination intensity = 0.6 W/cm^2 at the sample plane) was

synchronized with the intensifier component of an ICCD (Mega-10EX, Stanford Photonics, Inc.) such that a 10 μs delay was inserted between the end of the LED pulse and the intensifier start-time. For each acquisition, the signal from multiple excitation/emission events was accumulated on the ICCD sensor and read out at the end of the camera frame. The source/camera timing parameters were the same for all of the time-gated images and data presented here: excitation pulse width = 1500 μs, pulse period = 3000 μs, delay time = 10 μs, intensifier on-time = 1390 μs. The sensitivity of time-gated imaging is dependent on the number of excitation/detection events integrated on the CCD during a single camera frame and on the intensifier gain voltage. Frame summing was used to increase the signal-to-noise ratio and to remove ion-feedback noise from the intensifier. Each frame summed effectively increases the bit depth of the resulting image in increments of 1024 (i.e., 1 frame yields bit depth equal to 1024, 2 frames, 2048, etc.). ICCD images (tagged image file format, .TIF) were captured with the Piper control software (v2.4.05, Stanford Photonics, Inc.) and Axiocam images (.ZVI) were captured with the Zeiss AxioVision software (v4.6). All images were cropped and adjusted for contrast using NIH ImageJ (v1.34).

For quantitative analysis of Tb^{3+}-to-fluorescein LRET (Fig. 3c), two sets of time-gated images (λ_{em} = 520 nm and λ_{em} = 540 nm) were acquired for the same fields of view under identical exposure settings. Cells were selected for analysis from fields of view where the continuous wave fluorescein signal was either completely diffuse or completely punctate (2 separate experiments and 4 fields of view for each condition). The threshold tool in NIH ImageJ was used to

select regions of interest (ROI) in the time-gated images corresponding to the nuclei of luminescent cells. The emission signal intensity was calculated according to the equation: $S = (\mu_{signal}-\mu_{bckg})$, where, μ_{signal} is equal to the mean pixel gray value in an ROI corresponding to a luminescent nucleus, and μ_{bckg} is equal to the mean pixel gray value in a similarly sized ROI in a part of the image with no cells. The donor normalized LRET signal was defined as the ratio (S_{520}/S_{540}) of mean gray values from corresponding ROIs in each image pair. The mean and standard deviation of the LRET ratios for numerous cells representing each condition (diffuse and punctate) were then calculated.

3.2. Results and Discussion.

3.2.1. Peptide synthesis and characterization.

The peptide conjugates described in this study (**Figure 3.1**) were prepared as N-terminal fusions of either Lumi4 or a heterodimer of Lumi4 and a triethyleneglycolamino derivative of TMP (TEGTMP) to variations of Arg_9 or Tat. Lumi4 is an octadentate, macrotricyclic ligand with four, 2-hydroxyisopthalamide chelating units [113]. Its Tb^{3+} complex exhibits highly efficient emission (Φ_{total} > 50%), a large extinction coefficient ($\varepsilon_{max} \geq 20{,}000$ $M^{-1}cm^{-1}$ at λ = ~340 nm), and long luminescence lifetime (τ > 2.4 ms) in aqueous solutions. Following dissolution of lyophilized peptides in H_2O and addition of aqueous $TbCl_3$ solution, all conjugates exhibited characteristic terbium luminescence (**Figure 3.2**).

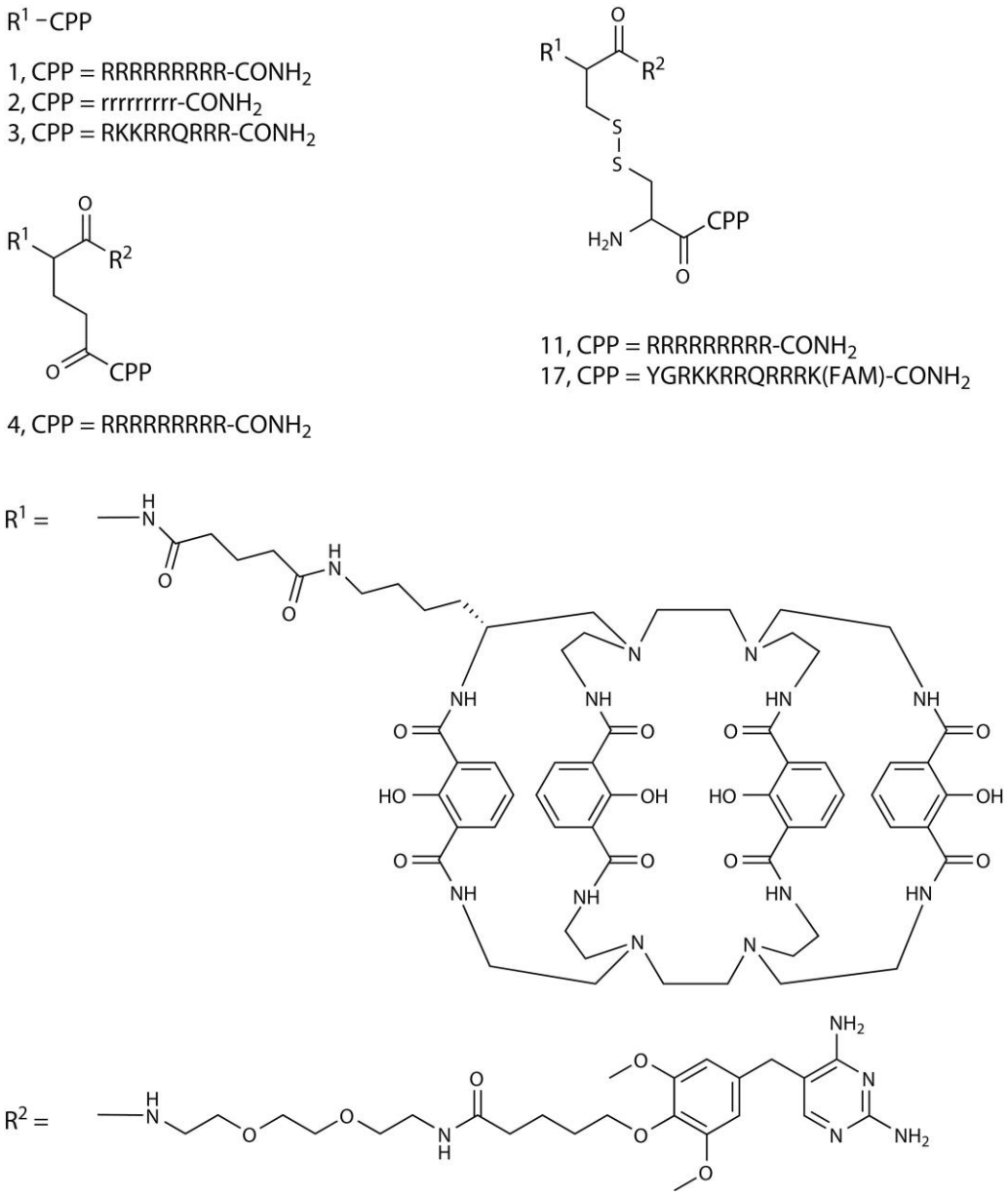

Figure 3.1. Chemical structures of the peptide conjugates used in this study. Abbreviations: R1, linker-functionalized derivative of Lumi4; R2, triethyleneglycolamino derivative of trimethoprim (TEGTMP); capital letters, L-amino acids; small letters, D-amino acids; FAM, 5,6-carboxyfluorescein.

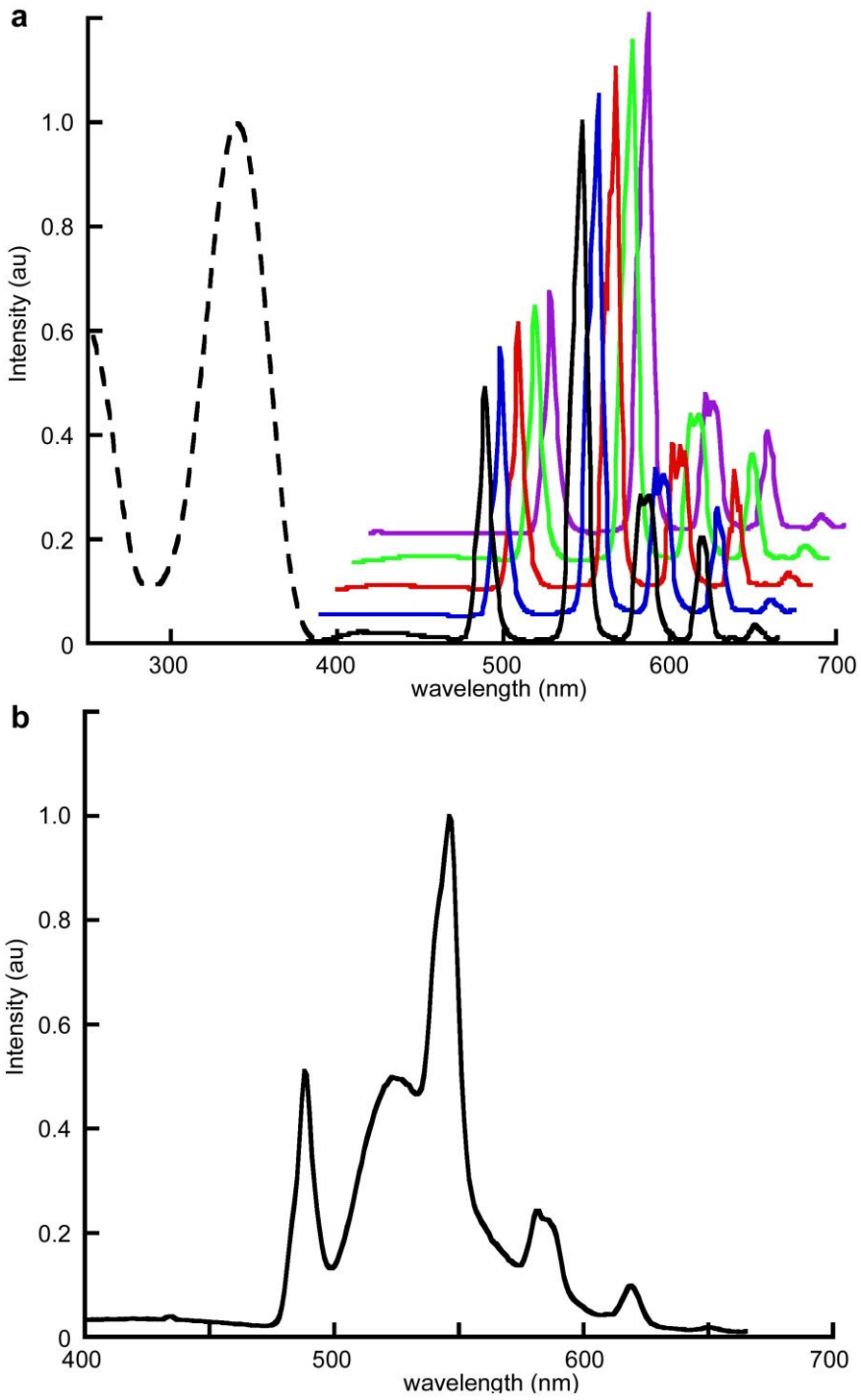

Figure 3.2. Emission spectra of luminescent lanthanide complexes in this study. **a**) Excitation spectrum of **1** (black, dotted) and emission spectra (solid) of **1** (black), **2** (blue), **3** (red), **4** (green) and **11** (purple). Emission spectra are vertically offset (0.05 a.u.) and horizontally offset (10 nm) for clarity. **b)** Emission spectrum of **17** showing mix of Tb^{3+} and fluorescein emission.

3.2.2. Effects of extracellular concentration and serum on uptake.

Peptide delivery, subcellular distribution, and specific labeling of eDHFR were assessed by using a previously described, time-gated microscope to visualize Tb^{3+} luminescence or LRET between Tb^{3+} and a short-lifetime fluorophore [101]. With time-gated imaging, a brief delay (10 μsec) is imposed between pulsed excitation and detection to eliminate short-lifetime fluorescence background. For peptides 1–4, we observed that the mode of uptake and the resultant cellular distribution depended on the extracellular peptide concentration, with apparent endocytosis occurring at relatively low concentrations, and direct translocation from culture medium to cytoplasm occurring at higher concentrations (**Figure 3.3a, top**). However, when MDCKII cells were incubated with higher peptide concentrations (20–60 μM) in complete medium, Tb^{3+} luminescence was observed throughout the cytoplasm and nucleus, suggesting direct translocation from culture medium to cytoplasm (**Figure 3.3a**, **bottom**). In addition, a similar uptake and subcellular distribution pattern of Lumi4-(L)-Arg_9 (**1**) was seen in various cell types including HeLa, NIH3T3 and HEK293 (**Figure 3.3 b**).

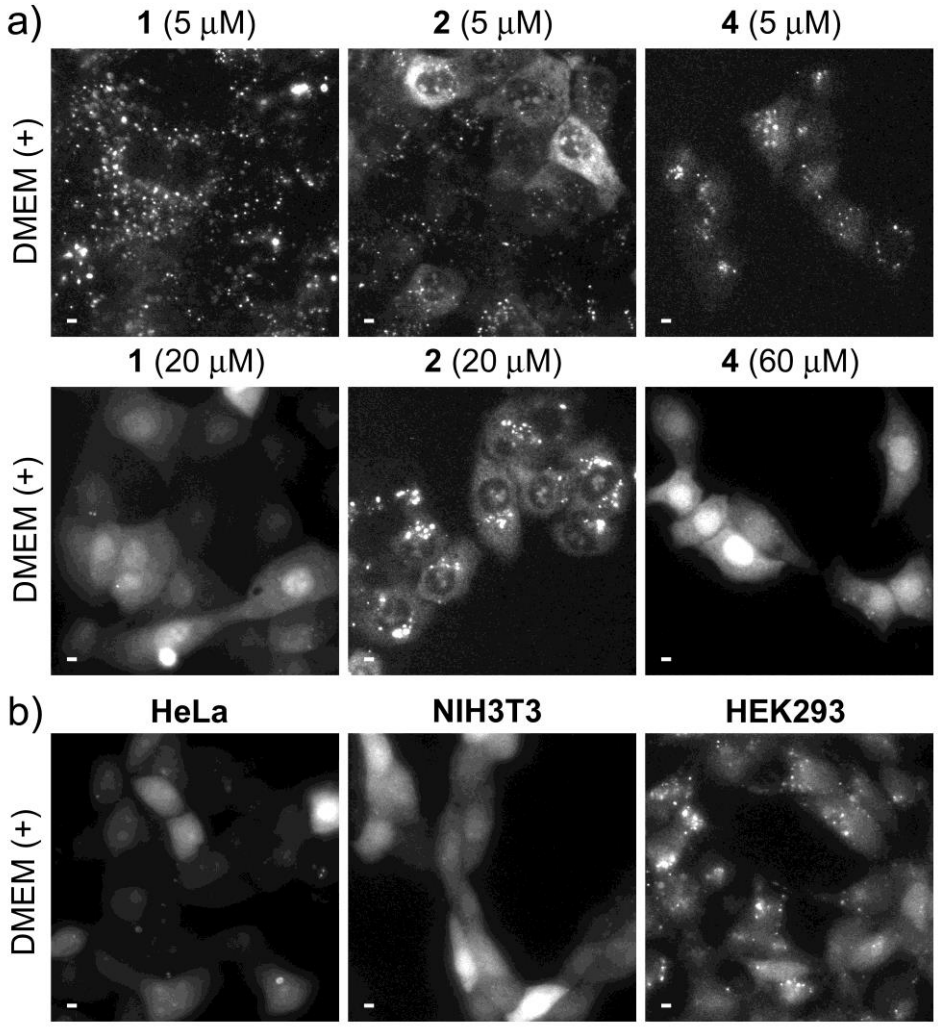

Figure 3.3 Effects of extracellular peptide concentration on uptake and distribution. Micrographs of time-gated luminescence (delay=10 μs, λ_{ex} = 365 nm, λ_{em} = 540 ± 10 nm); scale bars, 10 μm. **a)** MDCKII cells were incubated for 30 min at 37^0C in Dulbecco's modified Eagle's medium with FBS (DMEM (+)) that contained indicated concentrations of peptides **1**, **2** or **4.** Incubation in DMEM (+) containing low (5 μM) concentrations of indicated peptides results in punctate Tb^{3+} luminescence (top) whereas incubation in DMEM (+) above a threshold concentration (20 μM, **1**, **2**; 60 uM, **4**) results in diffuse distribution of Tb^{3+} luminescence throughout the cytoplasm and nucleus (bottom). **b)** Indicated cell types were incubated for 30 min. at 37 °C in DMEM (+) containing **1** (20 μM), washed 2X in PBS and re-immersed in DMEM (+) containing 1 mM Patent Blue™ prior to imaging.

3.2.3. Effects of temperature and serum on uptake.

It was further observed that incubation in medium without FBS lowered the threshold concentration for observing diffuse staining (**Figure 3.4, top**), presumably because Arg_9 binds to serum proteins, thus lowering its effective concentration in complete medium [114]. Similar results were seen when MDCKII cells were treated with conjugate **3**, an N-terminal fusion of Lumi4(Tb) to Tat (49–57) (not shown, reported in [111]). Although the distribution pattern seen at or above threshold levels was similar in different cells, the degree of uptake varied, with some cells appearing brightly luminescent and others showing little or no uptake. Although L-Arg_9 conjugates, **1** and **4**, distributed uniformly throughout the nucleus, the conjugate of Lumi4 to D-Arg_9 (**2**) exhibited a mix of punctate and diffuse staining, with nuclear luminescence confined to substructures. Observation of diffuse luminescence in MDCKII cells incubated at 4 °C in FBS-free medium containing **1**, **2**, or **4** (10 μM) further suggests that the uptake at higher effective concentrations occurs through an energy-independent, nonendocytic translocation mechanism (**Figure 3.4, bottom**).

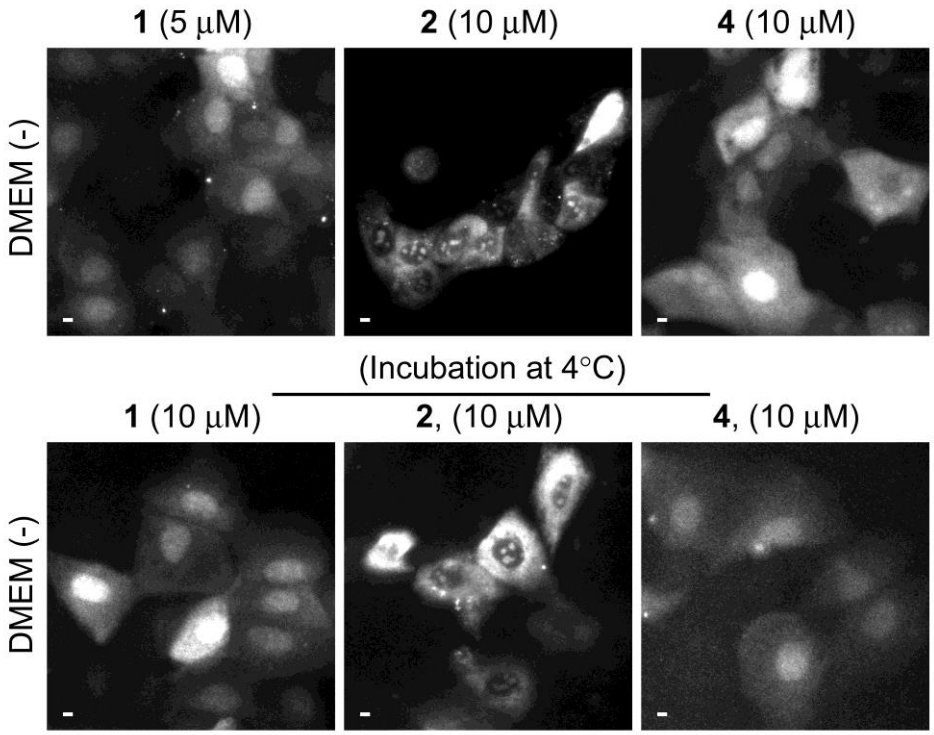

Figure 3.4. Effects of serum and temperature on uptake and distribution. Micrographs: time-gated luminescence (delay = 10 μs, λ_{ex} = 365 nm, λ_{em} = 540 ± 10 nm) Scale bars, 10 μm. MDCK cells were incubated for 30 min. at 37 °C (top) or 4 °C (bottom) in Dulbecco's modified eagle medium without fetal bovine serum (DMEM (-)) that contained indicated concentrations of peptides **1**, **2**, or **4**.

3.2.4. Effects of co-incubation with unconjugated Arg9.

Delivery into the cytoplasm and nucleus, as opposed to trapping in vesicles, is critical when delivering protein-targeted fluorophores as this allows access to a variety of targets. Another important factor is the ability to control the amount of label that is delivered. If too much is delivered, the target protein will be saturated and unbound label will lower the contrast seen in microscopic images. We were able to control intracellular delivery of terbium complex by incubating MDCKII cells in medium containing relatively high concentrations (30 μM) of unconjugated **Arg_9** with lower concentrations (5 μM) of conjugate Lumi4-L-$(Arg)_9$ (**1**). We observed uniform cytosolic and nuclear distribution of luminescence despite treatment with subthreshold concentrations of conjugated peptide (**Figure 3.5, left**). Moreover, 30-fold greater exposure times were needed to image terbium luminescence in co-labeled cells relative to cells that were incubated in high concentrations (20 μM) of conjugated peptide (**Figure 3.5, right**). These results suggest that cytoplasmic delivery depends on the total extracellular CPP concentration (unconjugated and cargo- linked), and this feature can be leveraged to deliver substoichiometric amounts of label relative to target protein levels.

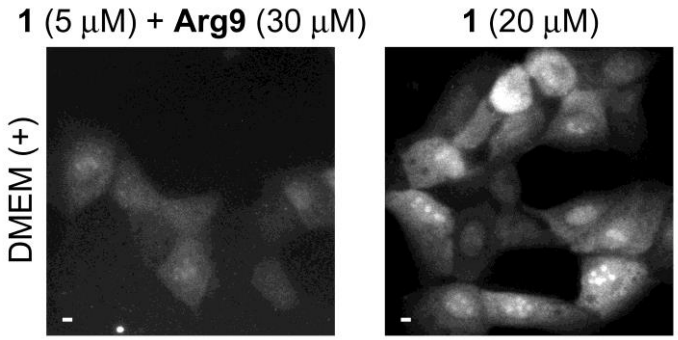

Figure 3.5. Effects of co-incubation with unconjugated Arg_9. Micrographs: time-gated luminescence (delay = 10 μs, λ_{ex} = 365 nm, λ_{em} = 540 ± 10 nm) Scale bars, 10 μm. Cells incubated in DMEM (+) containing **1** (5 μM) plus **Arg_9** (30 μM) show diffuse Tb^{3+} luminescence (left) similar to that seen in cells incubated in DMEM (+) containing higher concentrations of **1** (20 μM, right).

3.2.5. Visualization of specific binding of TMP-Lumi4 to eDHFR using time-gated microscopy.

We next sought to determine whether TMP conjugates could be passively delivered into cells for labeling of eDHFR fusion proteins. MDCKII cells were transiently transfected with DNA encoding a three-component protein chimera consisting of histone 2B linked to the red fluorescent protein TagRFP-T [112] and eDHFR (H2B–TagRFPT– eDHFR). Following incubation in serum-free medium containing **4** (10 uM), time-gated imaging (delay=10 μs, λ_{em}= 605/15) nm) of the Tb^{3+}-to-TagRFP-T LRET signal (**Figure 3.6b, left**) revealed nuclear luminescence that coincided with the steady-state fluorescence of TagRFP-T in express expressing cells (**Figure 3.6b, right**). When unconjugated TMP (final concentration ~100 mm) was added to the imaging medium, it diffused into cells,

competed with **4** for eDHFR binding, and eliminated nuclear luminescence (**Figure 3.6b, right**). These results and those above show that **4** translocates from culture medium into the cytoplasm of MDCKII cells, diffuses freely throughout the cytoplasm and nucleus and binds selectively to eDHFR. Successful labeling of H_2B– TagRFPT–eDHFR in MDCKII cells was also observed with **11**, a cysteine amide-linked heterodimer of Lumi4 and TEGTMP conjugated to $CysArg_9$ via a disulfide bond (**Figure 3.7**).

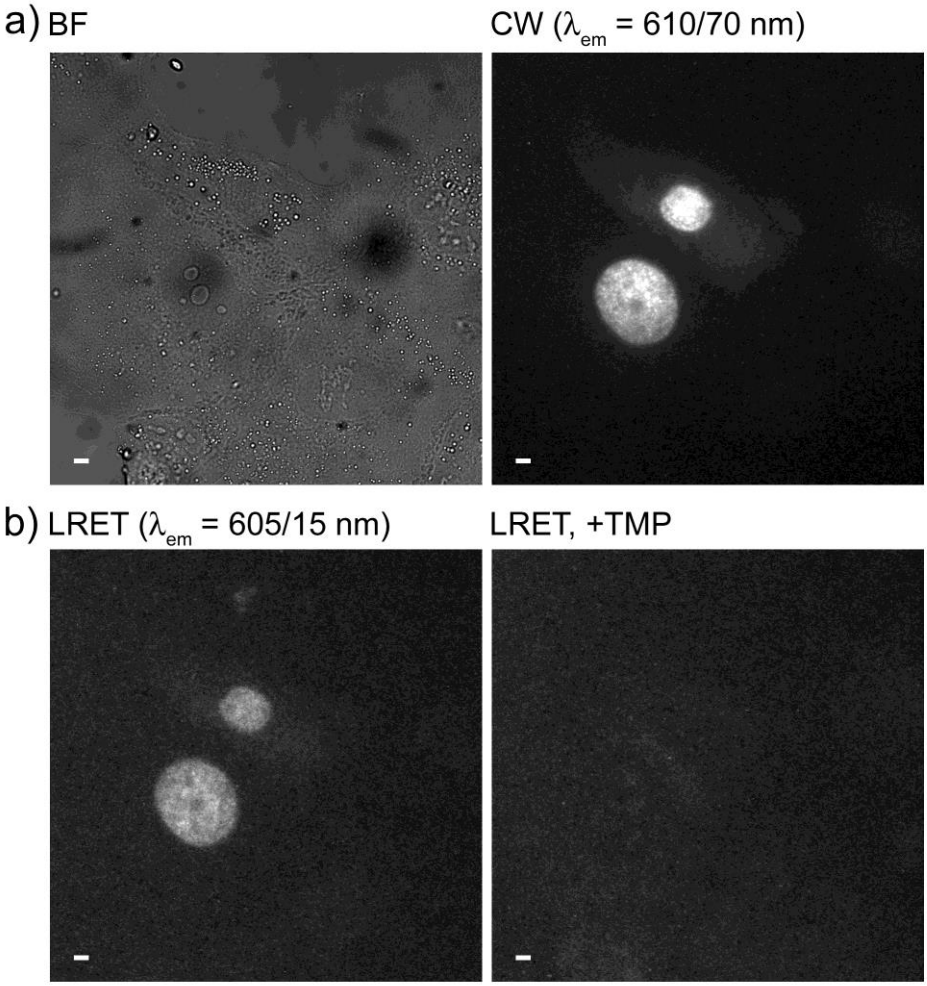

Figure 3.6. Arg_9 mediates cytoplasmic delivery of 4 **and specific labeling of H2B–TagRFPT–eDHFR as evidenced by time-gated LRET imaging of Tb^{3+}-to-TagRFP-T sensitized emission.** MDCKII cells transiently expressing H2B–TagRFPT–eDHFR were incubated for 30 min at 37°C in DMEM (-) containing **4** (10 (M), washed twice in PBS and re-immersed in DMEM (+) containing Patent Blue((1 mM) prior to imaging. a) Bright field (BF) and continuous wave (CW) fluorescence ((ex = 545 (15) nm, (em = 610 (35) nm) images reveal nucleus-localized TagRFP-T fluorescence in expressing cells. b) Time-gated LRET (delay=10 (s, (ex = 365nm, (ex = 605 (7 nm) image shows long-lived, Tb^{3+}-sensitized TagRFP-T emission (left) that disappears when TMP (final concentration= 100 (M) was added to medium (right); scale bars, 10 μm.

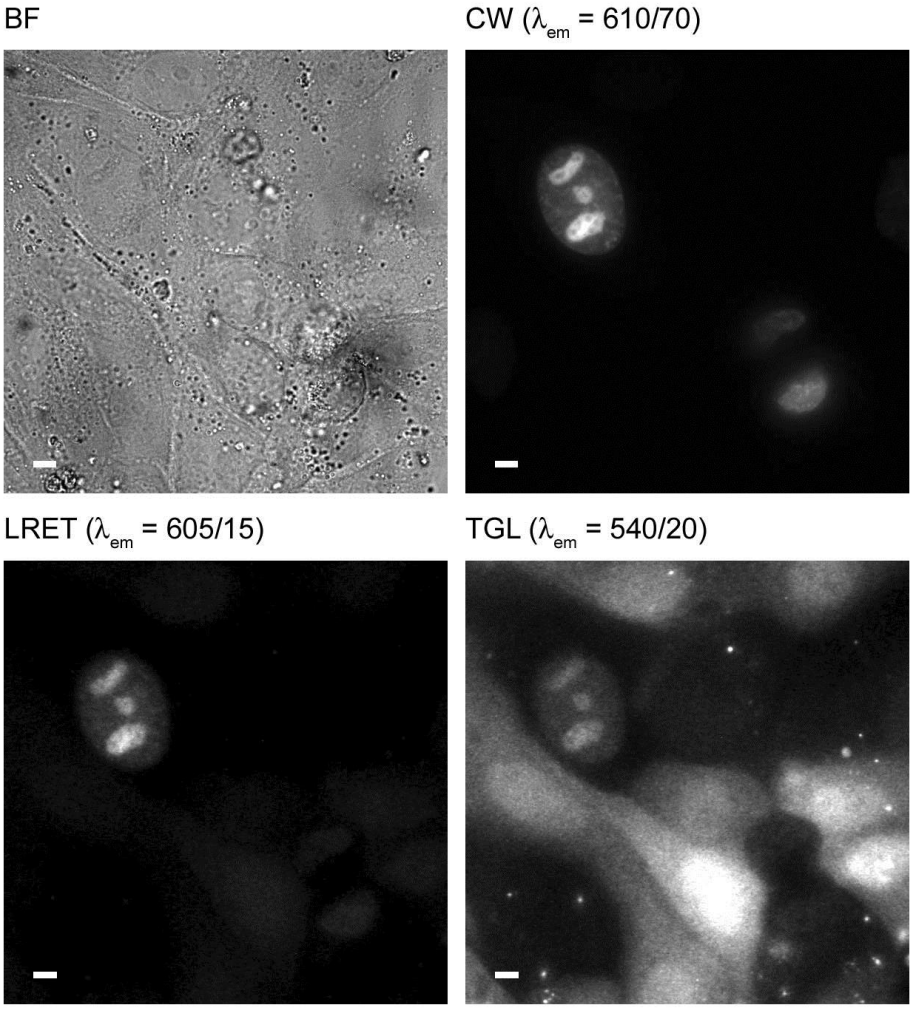

Figure 3.7. Arg_9 mediates cytoplasmic delivery of 11 **and specific labeling of H2B-TagRFPT-eDHFR as evidenced by time-gated LRET imaging of Tb^{3+}-to-TagRFP-T sensitized emission**. MDCK cells transiently expressing H2B-TagRFPT-eDHFR were incubated for 30 min. at 37 °C in DMEM (-) containing **11** (10 μM), washed 2X in PBS and re-immersed in DMEM (+) containing 1 mM Patent Blue™ prior to imaging. Micrographs: BF, bright field; CW, continuous wave fluorescence (λ_{ex} = 545 ± 15 nm, λ_{em} = 610 ± 70 nm); LRET, time-gated luminescence (delay = 10 μs, λ_{ex} = 365 nm, λ_{em} = 605 ± 15 nm); TGL, time-gated luminescence (delay = 10 μs, λ_{ex} = 365 nm, λ_{em} = 540 ± 10 nm). Scale bars, 10 μm.

3.2.6. Intracellular delivery and reductive cleavage of a disulfide bond between a CPP and its cargo.

We prepared Lumi4-Tb-Cys-Cys-Arg_9 (**11**) with the expectation that the disulfide bond would be cleaved by reducing agents (e.g., glutathione) in the cytoplasm or nucleus, thereby freeing the TMP–Lumi4 moiety for eDHFR binding. However, the luminescence phenotypes observed when **11** and **4** were used to label H2B–TagRFPT–eDHFR were essentially the same (**Figures 3.6, 3.7**), and disulfide reduction of **11** could not be confirmed microscopically. To assess the validity of our disulfide linker strategy, we prepared a cysteine amide-linked heterodimer of Lumi4 and TEGTMP and coupled this via a disulfide bond to the peptide Cys-TAT (47–57)-Lys (FAM). With this conjugate, **17**, we expected that the presence of a fluorescein moiety linked to the lysine side chain would make it possible to directly image disulfide reduction in live cells by quantifying the change in the intramolecular $Tb^{3+}$to-fluorescein LRET signal (**Figure 3.8**).

MDCKII cells were incubated in serum-free medium containing **17** (10 μM) for 10 min, washed with PBS, and imaged in continuous wave (fluorescein fluorescence, λ_{ex}=480 ± 40 nm), λ_{em} = 535 ± 50 nm) and time-gated modes (delay = 10 μs; Tb^{3+} luminescence, λ_{em} =540 ± 10 nm; Tb^{3+}-to-fluorescein LRET, λ_{em}=520 ± 10 nm). Immediately after being washed, the fluorescein signal in most cells was primarily diffuse throughout the cytoplasm and nucleus (**Figure 3.8a, top**). However, the fluorescein signal gradually redistributed into puncta that were located outside the nucleus, with the punctate staining pattern predominant 2 h

postwash (**Figure 3.8a, bottom**). Although the fluorescein signal redistributed, the Tb^{3+} luminescence remained diffuse throughout the cytoplasm and nucleus, and the Tb^{3+}-to-fluorescein LRET emission ratio (520/540 nm) was significantly reduced (**Figure 3.8 a, b**). These results show that **17** translocates directly into cells where its disulfide bond is reduced in the cytoplasm and nucleus. Upon reduction, the Lumi4- Cys-TEGTMP moiety diffuses freely throughout the cell whereas the Cys-Tat (49–57)-Lys (FAM) moiety redistributes to extranuclear structures via an undetermined mechanism. Although it is possible that the observed separation of the fluorescein and TMP–Lumi4(Tb) moieties results from proteolysis of the carrier peptide rather than disulfide reduction, this is unlikely because cleavage is complete within 120 min. A prior study found that proteolytic degradation of nonaarginine occurred in MDCK epithelial cells with a half-life of approximately 1400 min. [115].

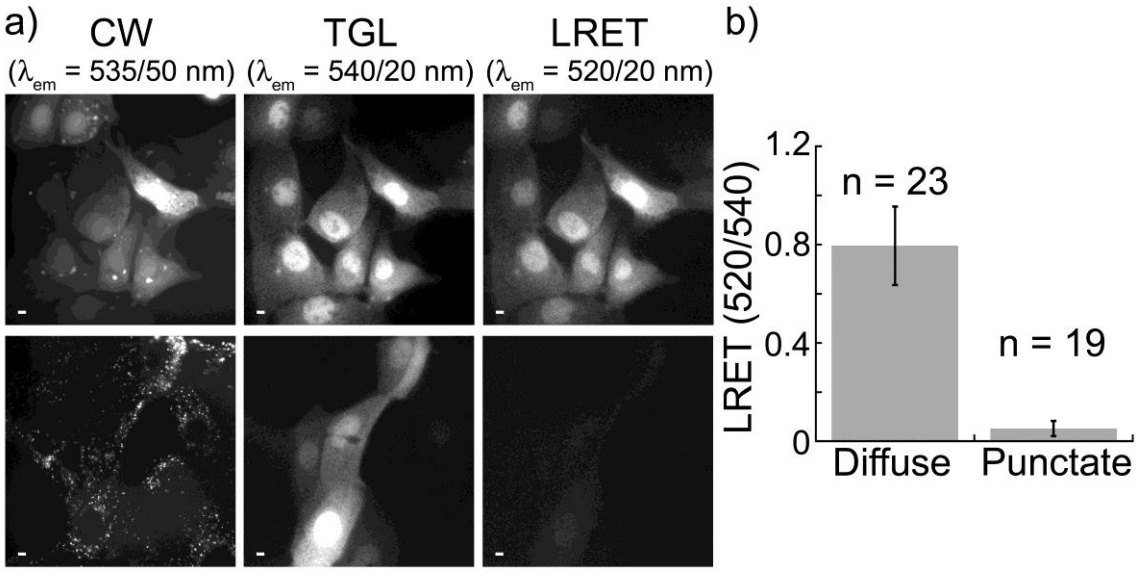

Figure 3.8. Intracellular disulfide reduction releases cargo from carrier peptide. MDCKII cells were incubated for 10 min at 37°C in DMEM (-) containing **17** (10 μM), washed twice in PBS and re-immersed in DMEM (+) containing Patent Blue (1 mM) prior to imaging. Micrographs: CW, continuous wave fluorescence (λ_{ex} = 480 ± 40 nm, λ_{em} = 535 ± 50 nm); TGL, time-gated luminescence (delay=10 μs, λ_{ex} = 365 nm, λ_{em} = 540 ± 10 nm); LRET, luminescence resonance energy transfer (delay = 10 μs, λ_{ex} = 365 nm, λ_{em} = 520 ± 10 nm). Scale bars, 10 μm. **a)** Top: representative images of cells acquired immediately following the wash step. Fluorescein fluorescence, Tb^{3+} luminescence, and Tb^{3+}-to-fluorescein LRET signals are diffuse throughout the cytoplasm and nucleus. Bottom: representative images of cells acquired approximately 2 h post-wash. Fluorescein signal is punctate whereas Tb^{3+} luminescence and diminished LRET signals remain diffuse. **b)** Mean, normalized, time-gated LRET signal (520/540 nm) measured in the nuclear region of cells exhibiting diffuse (immediate) and punctate (2 h post-wash) patterns of continuous wave, fluorescein fluorescence. Error bars represent standard deviation of the mean values (n = no. of cells) obtained from four separate experiments.

3. 3. Conclusion.

All of microscopic observations of CPP-mediated Tb^{3+} complex delivery (**Figures 3.3-3.8**), including concentration and serum dependence of uptake and distribution, cell-to-cell variability in uptake levels, temperature independence of high-concentration delivery and differences in distribution patterns of L- and D-peptides were consistent with earlier studies that examined the uptake of oligoarginines and Tat linked to fluorescein or AlexaFluor 488 [91, 114, 116]. These studies provided evidence that oligoarginines and Tat mediate low-concentration delivery of fluorophores into cells using three endocytic pathways: macropinocytosis, clathrin-mediated endocytosis and caveolae/lipid-raft-mediated endocytosis. Further, these studies show that uptake at higher concentrations occurs through direct translocation from medium to cytoplasm.

In this study, we observed that both Arg_9 conjugated at its N terminus to Lumi4 (**1**, **2**), Lumi4–GluTEGTMP (**4**) or Lumi4–CysTEGTMP (**11**) and Tat conjugated at its N terminus to Lumi4 (**3**) or Lumi4–CysTEGTMP (**17**) mediate non-endocytic, cytoplasmic delivery. Although cellular uptake of unconjugated and CPP-conjugated lanthanide complexes has been previously observed, [50, 98, 117-119] this is the first report of CPP-mediated, cytoplasmic delivery, and specific molecular targeting of an otherwise cell-impermeable probe. Selective, intracellular labeling of eDHFR fusion proteins with TMP–Lumi4 heterodimers should make it much easier to perform time-gated, LRET imaging of protein–protein interactions. Furthermore, the basic architecture of the conjugates described here, in which a ligand-label heterodimer is coupled directly to the N

terminus or via a disulfide linkage to an N-terminal cysteine residue of Arg_9 or Tat may be extended to other protein labeling systems, such as SNAP/CLIP-Tag or Halo-Tag [26, 120]. The fact that various fluorophores have been successfully delivered into live cells by N-terminal conjugation to arginine-rich peptides suggests that it should be possible to deliver cyanines, photosensitive dyes, or other high-performance labels for applications such as single molecule or superresolution imaging.

Chapter 4

CURRENT AND FUTURE DEVELOPMENT OF CELL-PENETRATING PEPTIDES FOR LIVE CELL PROTEIN LABELING AND IMAGING.

4. Introduction

The results presented in Chapter 3 offer a strategy for making chemical protein labeling live up to its full potential, where high-performance probes can be synthetically engineered and then selectively targeted to proteins in live cells in a controlled manner. Despite intense research focused on the development and characterization of CPPs as carriers for imaging and therapeutic agents, the idea of linking CPPs to a ligand-receptor heterodimer for selective labeling of recombinant proteins has hardly been explored. Only one example was reported prior to our study: Tsien and co-workers linked bis-arsenical fluorescein (FlAsH) to oligoarginine as a means of studying CPP uptake by FRET microscopy [1]. Nevertheless, our results demonstrataing direct translocation of nonaarginine-conjugated TMP-Lumi4 from culture medium to cytoplasm and subsequent binding to eDHFR in the nucleus suggest that other membrane-impermeant probes could be easily targeted to a wide variety of intracellular targets.

To assess the general usefulness of CPPs for chemical protein labeling in live cells, several questions must be answered:

- To what extent does the mechanism of cell entry and resulting sub-cellular distribution depend on the cargo?
  - Can other protein targeting ligands besides TMP be used, such as SNAP-Tag, CLIP-Tag or Halo-Tag?
  - What other varieties of probes can be used (e.g., cyanines, photoactivateable dyes)?

- How well can the intracellular concentration of CPP-delivered cargo be controlled?
- To what extent does cell type or cell culture/labeling conditions affect the mode of entry.
- What is the rate of direct translocation from culture medium to cytoplasm, and can this be controlled?

In this chapter, the results of some preliminary studies addressing the above questions are presented. Cytoplasmic delivery of nonaarginine-conjugated, benzyl guanine-Lumi4 and benzyl-cytosine-Lumi4 heterodimers and covalent binding to their respective substrates (SNAP-Tag, CLIP-tag) is demonstrated using time-gated microscopy. Additional results showing real-time uptake of TMP-Lumi4-Arg_9 into MDCK cells as well as the temperature dependence of uptake mechanism in different cell lines is presented. These studies are ongoing in the Miller laboratory, and a perspective on future work in this area is offered.

4.2. Experimental Methods.

4.2.1. Materials and analyses.

All chemicals were obtained from Sigma-Aldrich, Inc., and cell culture reagents were purchased from Invitrogen, Inc. Cysteine amide-linked heterodimers of Lumi4 and triethyleneglycolamino-benzyl guanine and triethyleneglycolamino-benzyl cytosine conjugated to $CysArg_9$ (Lumi4-SNAP-$CysArg_9$ and Lumi4-CLIP-$CysArg_9$, respectively) were prepared by Darren

Magda at Lumiphore, Inc. H2B-SNAP and H2B-CLIP plasmids were purchased from New England Biolabs, Inc. MDCKII cells were provided by Prof. J.R. Turner.

4.2.2. Cell Culture and Transfection.

MDCKII cells were cultured in DMEM (+) (Dulbecco's Modified Eagle Media supplemented with 10% FBS, 2 mM L-glutamine, 100 unit⁄mL penicillin and 100 μg⁄mL of streptomycin) at 37 °C and 5% CO_2. MDCK cells were seeded at 10^5 cells per well into a 6-well plate. After ~18 h incubation at 37 °C and 5% CO_2, adherent cells (~80% confluent) were transfected with 2 μg of the H2B-SNAP or H2B-CLIP (New England Biolabs) and CFP using Lipofectamine2000™ (Invitrogen) according to manufacturer's instructions. Approximately 6 h after transfection, cells were trypsinized and reseeded at 15,000 cells⁄well into 8-well chambered coverglasses (Nunc™, 12-565-470) and incubated at 37 °C and 5% CO_2 overnight. An MDCKII cell line that stably expresses H2B-GFP-eDHFR was prepared by Megha Rajendran by clonal selection with G418. Experiments using non-transfected, transiently transfected or stably transfected cells were performed following seeding at 15,000 cells⁄well into 8-well chambered coverglasses and overnight incubation at 37 °C and 5% CO_2.

4.2.3. Microscopy image acquisition.

Peptide delivery, sub-cellular distribution, and specific labeling of recombinant receptor fusions were assessed using time-gated microscopy to visualize Tb^{3+} luminescence or LRET between Tb^{3+} and a GFP, as described in Chapter 3 [2]. Images (.TIFF) were analyzed using NIH ImageJ.

4.2.4. Peptide Internalization protocol

For labeling with peptides, cells growing in DMEM (+) in 8-well chambered coverglasses were washed 1X with PBS and re-immersed in DMEM (-) (same as DMEM (+) without FBS) at the desired temperature (37 °C or 22 °C) containing peptides at the indicated concentration. Cells were then incubated at 37 °C and 5% CO_2 (in ambient atmosphere for 22 °C studies), washed 2X in PBS and reimmersed in DMEM (+) supplemented with 1 mM Patent Blue™ dye to quench extracellular luminescence.

4.3. Results and Discussion.

4.3.1. Intracellular delivery of Lumi4-SNAP-Arg9 and Lumi4-CLIP-Arg9 and labeling of H2B-SNAP/CLIP.

SNAP-Tag™ and CLIP-Tag™ are small (~22 kDa) proteins engineered from O^6-alkylguanine-DNA alkyltransferase (hAGT), a DNA repair protein. Benzyl guanine and benzyl cytosine react with SNAP and CLIP respectively to form stable thioether linkages to reactive cysteine residues on the proteins [121]. Heterodimers of benzyl guanine or benzyl cytosine and fluorophores can thus be

used to covalently label appropriate hAGT fusion proteins in live cells. Using heterodimers of benzyl guanine and benzyl cytosine linked to Lumi4 and conjugated to $CysArg_9$ (Lumi4-SNAP-$CysArg_9$, Lumi4-CLIP-$CysArg_9$, **Figure 4.1**), we sought to determine whether H_2B-SNAP and H2B-CLIP could be labeled in live MDCKII cells following passive, CPP-mediated intracellular delivery.

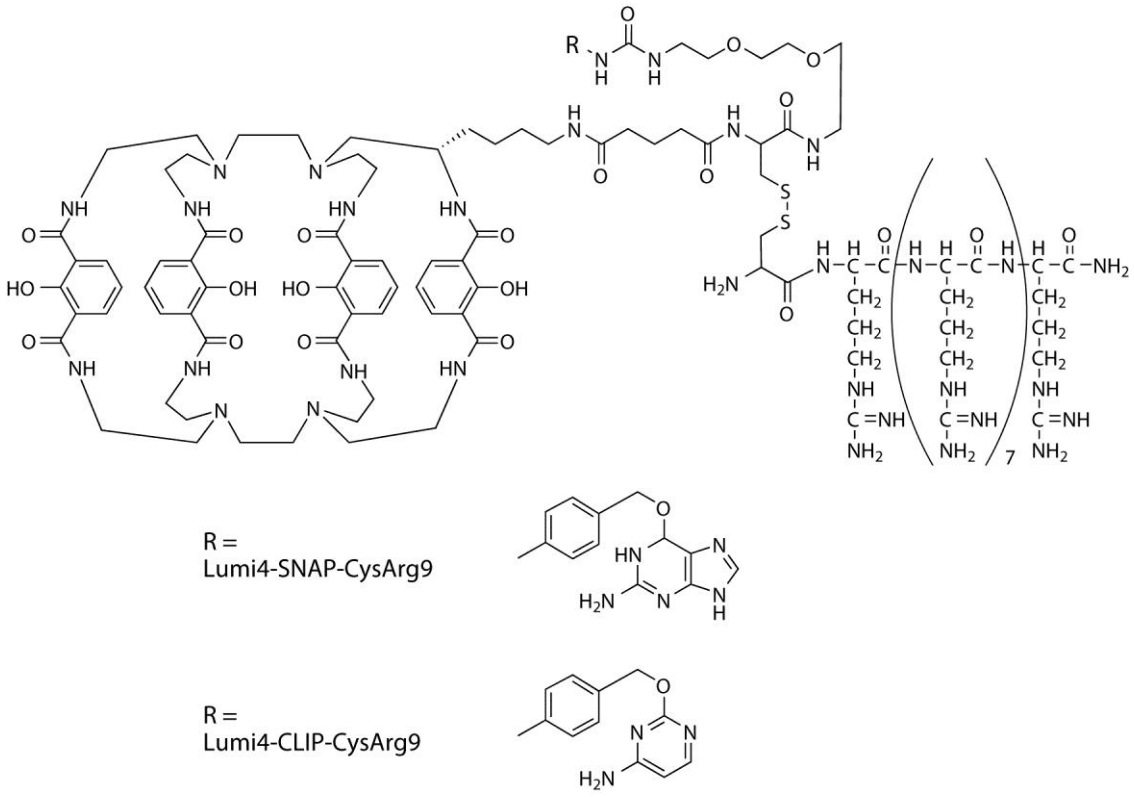

Figure 4.1. Chemical structure of Lumi4-SNAP-$CysArg_9$ and Lumi4-CLIP-$CysArg_9$.

Prior to labeling studies, we first simply tested whether Lumi4-SNAP/CLIP reagents would translocate directly from the extracellular medium to cytoplasm in a manner similar to that seen with Lumi4 and TMP-Lumi4 conjugated to Arg_9 or Tat. When MDCK cells were incubated for 30 min. in

serum-free growth medium (DMEM (-)) containing either reagent (10 μM), diffuse Tb^{3+} luminescence was observed in >50% of cells. The effective incubation concentration of labeled reagents could be made lower by co-incubation with unconjugated Arg_9, as was observed for Lumi4 conjugated directly to the N-terminus of Arg_9 in Chapter 3 [4]. A representative image showing MDCK cells co-incubated with either Lumi4-SNAP-$CysArg_9$ or Lumi4-CLIP-$CysArg_9$ (3 μM) and unconjugated Arg_9 (60 μM) is shown in **Figure 4.2a.** These results suggest that there is some flexibility with respect to the cargo-dependence of CPP-mediated delivery, and that a variety of protein tagging technologies can be adapted to this method.

We next attempted to observe specific labeling of SNAP or CLIP tags in cells with their respective substrates. To do so, MDCK cells were transiently co-transfected with either H2B-SNAP or H2B-CLIP and a plasmid encoding Cyan Fluorescent Protein (CFP) linked to a nucleus localization sequence as a transfection marker. In this case, we hypothesized that intracellular delivery of sub-stoichiometric amounts of substrates relative to overexpressed target proteins would result in the majority of Lumi4 being bound to H_2B-SNAP or H_2B-CLIP in the nucleus, and this would result in a predominantly nuclear distribution of Tb^{3+} luminescence in transfected cells loaded with probe. It proved difficult to observe this result, and only few cells transfected with H2B-SNAP and loaded with Lumi4-SNAP-CysArg9 exhibited the expected pattern of luminescence (**Figure 4.2b**). Specific labeling of H_2B-CLIP with Lumi4-CLIP-$CysArg_9$ was not observed.

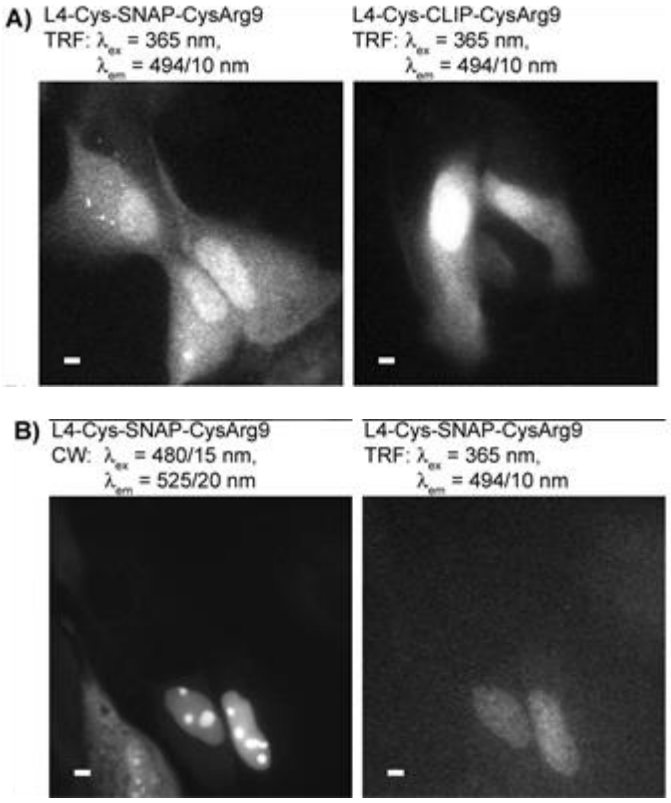

Figure 4.2. Cytoplasmic delivery of Lumi4-SNAP-CysArg$_9$ and Lumi4-CLIP-CysArg$_9$. a) MDCKII cells were incubated with indicated reagents (3 μM + 60 μM Arg$_9$ in DMEM (-), 37^{0}C) for 20 min., washed and imaged. Time-gated imaging (delay = 10 μs) shows diffuse Tb^{3+} luminescence throughout cytoplasm and nucleus, suggesting a direct translocation mode of cell delivery. **b)** MDCKII cells transiently co-transfected with plasmids encoding nucleus-localized CFP and H2B-SNAP. Co-localization of CFP fluorescence (left) and Tb^{3+} luminescence (right) in transfected cells suggest specific labeling of H2B-SNAP with Lumi4-SNAP-CysArg$_9$. Micrographs: (left) continuous wave fluorescence; (right) time-gated luminescence (delay =

Despite our attempt to deliver low concentrations of luminescent probes into cells by co-incubating with unconjugated Arg_9 (3 μM Lumi4-SNAP/CLIP-CysArg9, 60 μM Arg_9), we nevertheless observed considerable variation in the intracellular probe concentration following delivery. Many cells did not take up the probes at all, and many of the transfected cells showed Tb^{3+} luminescence throughout the cytoplasm and nucleus. This variation, combined with poor transient transfection efficiency (<10%) made it impossible to conclusively determine whether the Lumi4-linked substrates were binding to their targets. To better assess specific labeling of SNAP/CLIP proteins, H2B-GFP-SNAP and H2B-GFP-CLIP are being prepared that will make it possible to visualize specific, intracellular labeling by detecting Tb^{3+}-to-GFP LRET signals, as was done for TMP-Lumi4 in Chapter 3.

4.3.2. Cellular uptake behavior of Lumi4-TEGTMP-CysArg$_9$ in stably transfected MDCK cells.

Because practical use of CPP-delivery for intracellular protein labeling will require well- defined assay conditions, we quantitatively studied the uptake of CPP-linked terbium probes. Our goal is to simultaneously control the mode of uptake (i.e., ensure direct translocation while minimizing endocytosis) and the final intracellular concentration of cargo. To enable these studies, an MDCK cell line that stably expresses H2B-GFP-eDHFR was prepared by Megha Rajendran. With these cells, we hoped to eliminate cell-to-cell variability in protein expression with the expectation that we would be able to more easily obtain

statistically significant microscopy results. Time-gated imaging of Tb^{3+} luminescence and Tb^{3+}-to-GFP LRET signals in cells stably expressing H2B-GFP-eDHFR that are labeled with Lumi4-TEGTMP-$CysArg_9$ should make it possible to quantitatively determine 1) the relative proportions of cells that undergo direct translocation under a given set of incubation conditions; 2) the incubation conditions that deliver sub-stoichiometric amounts of probe relative to intracellular protein concentration (by comparing Tb^{3+} and LRET signals); and 3) the rate of peptide uptake for a given set of incubation conditions (by observing LRET signal changes in real-time in the presence of probe).

Our first experiment showed that stably transfected MDCK cells exhibit different behavior than non-transfected cells with respect to mode of uptake. When incubated at 37°C in DMEM(-) containing 10 μM Lumi4-TEGTMP-$CysArg_9$, the majority of non-transfected MDCK cells exhibit diffuse Tb^{3+} luminescence throughout, consistent with a direct translocation uptake mechanism (**Figure 4.3a**). However, the stably transfected MDCK cells exhibit a punctate pattern of Tb^{3+} luminescence, consistent with an endocytic uptake mechanism when treated under the same conditions (**Figure 4.3b**). We had previously observed that direct translocation as a mode of uptake was favored in cells that were passaged relatively few times. Since stable transfection requires many rounds of passaging and clonal selection, this result is not entirely surprising. What was unexpected, however, was that by incubating stably transfected MDCK cells at room temperature (~22°C), we were able to favor the direct translocation

mechanism, and nearly all cells exhibited diffuse Tb^{3+} luminescence and robust Tb^{3+}-to-GFP signals in the nucleus (**Figure 4.3c**).

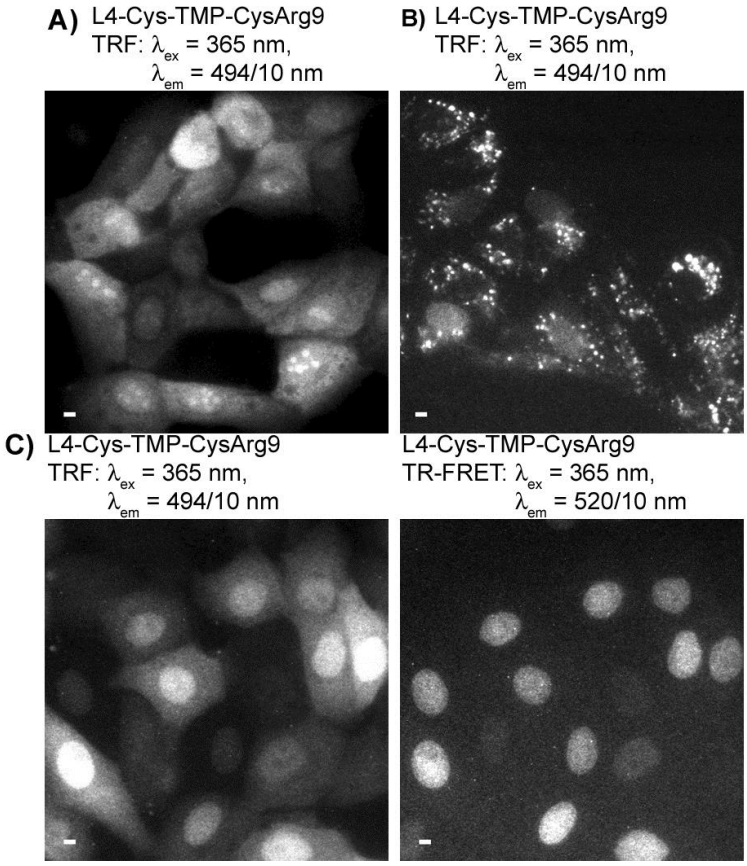

Figure 4.3. Uptake of Lumi4-TEGTMP-CysArg$_9$ in MDCKII cells is dependent on passage number and temperature. MDCKII cells were incubated with Lumi4-TEGTMP-CysArg9 (10 μM in DMEM (-), 20 min.), washed and imaged. Non-transfected cells (**a**) and cells stably transfected with H2B-GFP-eDHFR (**b**) show different sub-cellular distribution of Tb^{3+} luminescence when incubated at 37°C. **c**) Incubation at 22°C allows for direct translocation of probe into stably transfected cells as evidenced by diffuse Tb^{3+} luminescence and clear Tb^{3+}-to-GFP TR-FRET signals in nucleus (right). Scale bars, 10μm.

How to explain these results? First, while it is firmly established that direct translocation of arginine-rich peptides occurs, the mechanism of this process is not well understood. Biophysical evidence suggests that direct translocation is related to hydrogen bonding between guanidinium moieties of arginines and membrane lipids [122]. Furthermore, TAT peptides can induce pores in artificial membranes, and molecular-dynamics simulations suggest arginine-rich peptides can form transient pores in membranes in the presence of an electrochemical gradient, thus giving a mechanistic hypothesis for direct membrane translocation [123]. Moreover, a recent study showed that the direct translocation of nonaarginine depends on an induced translocation of acid sphingomyelinase to the outer leaflet of the plasma membrane and subsequent ceramide formation [124]. Thus, biological as well as biophysical mechanisms are implicated for direct translocation of CPPs. Therefore, it is not surprising to see that the mode of uptake is dependent not only on cell type, but also passage number and temperature, as these factors could affect both biochemical composition and physical properties (e.g., fluidity) of the cell membrane. From a practical standpoint, what is encouraging is that we can favor direct translocation over endocytosis by relatively simple changes in incubation conditions.

4.3.3. Real-time monitoring of Lumi4-Arg_9 uptake into MDCK cells.

We prepared the MDCKII cell line that stably expresses H2B-GFP-eDHFR as a tool to monitor uptake of CPP-linked TMP-Lumi4 in real-time using time-gated FRET microscopy [2]. However, at the time these experiments were

performed, the Lumi4-TEGTMP-CysArg$_9$ reagent was in short supply. Therefore, we visualized uptake of Lumi4-(L)-Arg$_9$ (compound **1** from Chapter 3) into the stably transfected MDCK cells by monitoring cellular Tb^{3+} luminescence without first washing the cells. Cells growing in an 8-well chambered coverslip were focused on the microscope stage at room temperature. Lumi4-(L)-Arg$_9$ was added into growth medium (estimated conc. 10 μM), and images were taken at various time-points. While the presence of saturated regions in the luminescence image is distracting, we can nevertheless observe that luminescence first becomes apparent at the cell membrane (within ~10 min.), and thereafter, the cytoplasm becomes increasingly bright (**Figure 4.4**). After 60 min. incubation followed by washing with Patent Blue (1 mM) to quench extracellular luminescence, the majority of cells appear uniformly luminescent throughout the cytoplasm.

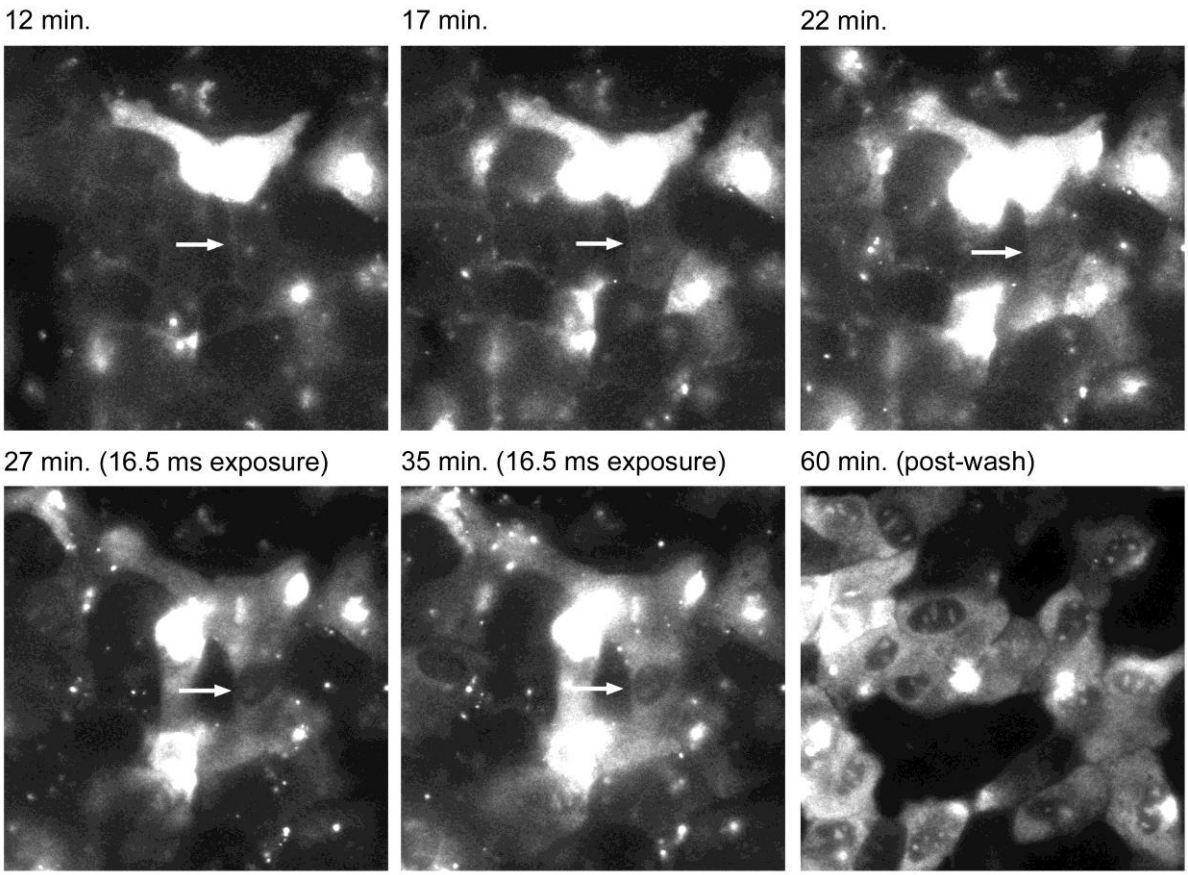

Figure 4.4. Time-lapse imaging of Lumi4-(L)-Arg$_9$ entry into stably transfected MDCK cells. MDCKII cells stably expressing H2B-GFP-eDHFR were incubated in DMEM(-) containing Lumi4-(L)-Arg$_9$ (10 μM, 22°C) and imaged without washing. Micrographs: time-gated luminescence (λ_{ex} = 365 nm, λ_{em} = 540 ± 20 nm, delay = 10 μs).

The rapid uptake into the cytoplasm seems to further support a mechanism where Lumi4-(L)-Arg_9 directly translocates into the cytoplasm (under appropriate conditions). Moreover, this result is consistent with those reported in a study that followed real-time uptake of nonaarginine conjugated to fluorescein using confocal microscopy [91]. In that study and others [79, 116] direct cytoplasmic import of oligoarginine occurred through spatially confined plasma membrane regions while plasma membranes remained intact. While supporting the direct translocation mechanism, observation of real-time changes in cellular Tb^{3+} luminescence has some limitations, and the results raise further questions. First, there is an abundance of bright puncta in the pre-wash images (**Figure 4.4**) that could indicate membrane-bound probe, internalized vesicles containing probe, or simply aggregates of probe molecules in the growth medium. Real-time FRET imaging would better resolve the difference between cytoplasmic/nuclear and extracellular signals. Secondly, the pattern of luminescence seen in the stably transfected cells incubated at room temperature with the Lumi4-(L)-Arg_9 (**Figure 4.4**, lower right image) resembles that seen when non-transfected MDCK cells are incubated with Lumi4-(D)-Arg_9 at 37°C, with diffusely bright cytoplasm and darker nuclei with punctate sub-structures (see **Figure 3.3a**). Thus, while altering incubation temperature directs Arg_9 conjugates to the cytoplasm in stably transfected cells, the mechanism of entry seems to be subtly different.

4.4. Conclusion.

These results indicate that Lumi4-peptide conjugates will be useful for a variety of experimental conditions. Time-resolved fluorescence (TRF) microscopic imaging of various TMP-Lumi4-Tb conjugated to cell-penetrating peptides showed that these peptides have a strong potential to be used as delivery vector for lanthanide imaging probes in less than few minutes. These studies are ongoing in the Miller laboratory, and a perspective on future work in this area is suggesting possible delivery of impermeant cyanines, photosensitive dyes, or other high-performance labels for applications such as single molecule or superresolution imaging [125, 126]. To summarize, these new studies on Lumi4-peptide conjugates should improve delivery of impermeant and photosensitive dyes which are widely used in single-molecule studies. For example, combining this technology with other impermeable imaging agents such as Cy3, and Cy 5, which are widely used in single-molecule experiments, allow researchers to quantify the photobleaching behavior of single-molecules.

Likewise, real-time single-molecule analysis implementing arginine-rich peptide base probes reveals more details about the mode of uptake of these CPPs suggesting multimechanism uptake process or a mechanism different from passive diffusion and endocytosis [126]. Moreover, it is very helpful to validate these peptide based cell penetrating imaging probes for superresolution microscopy studies such as identifying apoptotic cells in vivo applications that requires non-invasive molecular imaging probes. One strategy to assess apoptosis in vivo has been through the use of probes targeting extracellular or cell

membrane targets, such as the binding of reporter-labeled annexin V to phosphatidylserine exposed on the outer leaflet of the plasma membrane of apoptotic cells. One potential drawback to this strategy is that it may not adequately distinguish apoptotic from necrotic forms of cell death in vivo without a secondary marker of membrane integrity. It is anticipated that this strategy may have potential for use in humans in the diagnosis and management of glaucoma activatable probe for the near-infrared detection of apoptosis [127].

Thus, the cell-penetrating sequence serves both as a targeting sequence for selective cell accumulation of the probe and as a mediator of cell penetration. These ideas are ongoing studies in the Miller laboratory and a perspective on future work in this area is suggested.

REFERENCES

1. Xie, X.S., J. Yu, and W.Y. Yang, *Living cells as test tubes.* Science, 2006. **312**(5771): p. 228-30.
2. Wang, Y., J.Y. Shyy, and S. Chien, *Fluorescence proteins, live-cell imaging, and mechanobiology: seeing is believing.* Annu Rev Biomed Eng, 2008. **10**: p. 1-38.
3. Parekh, A.B. and R. Penner, *Store depletion and calcium influx.* Physiol Rev, 1997. **77**(4): p. 901-30.
4. Harootunian, A.T., et al., *Fluorescence ratio imaging of cytosolic free Na+ in individual fibroblasts and lymphocytes.* J Biol Chem, 1989. **264**(32): p. 19458-67.
5. Giepmans, B.N., et al., *The fluorescent toolbox for assessing protein location and function.* Science, 2006. **312**(5771): p. 217-24.
6. Tsien, R.Y., *The green fluorescent protein.* Annu Rev Biochem, 1998. **67**: p. 509-44.
7. Lichtman, J.W. and J.A. Conchello, *Fluorescence microscopy.* Nat Methods, 2005. **2**(12): p. 910-9.
8. Huang, B., M. Bates, and X. Zhuang, *Super-resolution fluorescence microscopy.* Annu Rev Biochem, 2009. **78**: p. 993-1016.
9. Joo, C., et al., *Advances in single-molecule fluorescence methods for molecular biology.* Annu Rev Biochem, 2008. **77**: p. 51-76.
10. Suhling, K., P.M. French, and D. Phillips, *Time-resolved fluorescence microscopy.* Photochem Photobiol Sci, 2005. **4**(1): p. 13-22.
11. Wallrabe, H. and A. Periasamy, *Imaging protein molecules using FRET and FLIM microscopy.* Curr Opin Biotechnol, 2005. **16**(1): p. 19-27.
12. Jing, C. and V.W. Cornish, *Chemical tags for labeling proteins inside living cells.* Acc Chem Res, 2011. **44**(9): p. 784-92.
13. Medintz, I.L., et al., *Quantum dot bioconjugates for imaging, labelling and sensing.* Nat Mater, 2005. **4**(6): p. 435-46.
14. Michalet, X., et al., *Quantum dots for live cells, in vivo imaging, and diagnostics.* Science, 2005. **307**(5709): p. 538-44.
15. Miller, L.W. and V.W. Cornish, *Selective chemical labeling of proteins in living cells.* Curr Opin Chem Biol, 2005. **9**(1): p. 56-61.
16. Wombacher, R. and V.W. Cornish, *Chemical tags: applications in live cell fluorescence imaging.* J Biophotonics, 2011. **4**(6): p. 391-402.
17. Griffin, B.A., S.R. Adams, and R.Y. Tsien, *Specific covalent labeling of recombinant protein molecules inside live cells.* Science, 1998. **281**(5374): p. 269-72.
18. Adams, S.R., et al., *New biarsenical ligands and tetracysteine motifs for protein labeling in vitro and in vivo: synthesis and biological applications.* J Am Chem Soc, 2002. **124**(21): p. 6063-76.
19. Marek, K.W. and G.W. Davis, *Transgenically encoded protein photoinactivation (FlAsH-FALI): acute inactivation of synaptotagmin I.* Neuron, 2002. **36**(5): p. 805-13.
20. Luedtke, N.W., et al., *Surveying polypeptide and protein domain conformation and association with FlAsH and ReAsH.* Nat Chem Biol, 2007. **3**(12): p. 779-84.
21. Gaspersic, J., et al., *Tetracysteine-tagged prion protein allows discrimination between the native and converted forms.* FEBS J, 2010. **277**(9): p. 2038-50.
22. Hu, Y., et al., *A strategy for designing a peptide probe for detection of beta-amyloid oligomers.* Chembiochem, 2010. **11**(17): p. 2409-18.

23. Ignatova, Z. and L.M. Gierasch, *Monitoring protein stability and aggregation in vivo by real-time fluorescent labeling.* Proc Natl Acad Sci U S A, 2004. **101**(2): p. 523-8.
24. Sun, X., et al., *Development of SNAP-tag fluorogenic probes for wash-free fluorescence imaging.* Chembiochem, 2011. **12**(14): p. 2217-26.
25. Banala, S., et al., *A caged, localizable rhodamine derivative for superresolution microscopy.* ACS Chem Biol, 2012. **7**(2): p. 289-93.
26. Gautier, A., et al., *An engineered protein tag for multiprotein labeling in living cells.* Chem Biol, 2008. **15**(2): p. 128-36.
27. Keppler, A., et al., *Labeling of fusion proteins with synthetic fluorophores in live cells.* Proc Natl Acad Sci U S A, 2004. **101**(27): p. 9955-9.
28. Maurel, D., et al., *Photoactivatable and photoconvertible fluorescent probes for protein labeling.* ACS Chem Biol, 2010. **5**(5): p. 507-16.
29. Keppler, A., et al., *A general method for the covalent labeling of fusion proteins with small molecules in vivo.* Nat Biotechnol, 2003. **21**(1): p. 86-9.
30. Farr, G.A., et al., *Membrane proteins follow multiple pathways to the basolateral cell surface in polarized epithelial cells.* J Cell Biol, 2009. **186**(2): p. 269-82.
31. Kropf, M., et al., *Subunit-specific surface mobility of differentially labeled AMPA receptor subunits.* Eur J Cell Biol, 2008. **87**(10): p. 763-78.
32. Maurel, D., et al., *Cell-surface protein-protein interaction analysis with time-resolved FRET and snap-tag technologies: application to GPCR oligomerization.* Nat Methods, 2008. **5**(6): p. 561-7.
33. Chen, I., et al., *Site-specific labeling of cell surface proteins with biophysical probes using biotin ligase.* Nat Methods, 2005. **2**(2): p. 99-104.
34. Howarth, M., et al., *Targeting quantum dots to surface proteins in living cells with biotin ligase.* Proc Natl Acad Sci U S A, 2005. **102**(21): p. 7583-8.
35. Uttamapinant, C., et al., *A fluorophore ligase for site-specific protein labeling inside living cells.* Proc Natl Acad Sci U S A, 2010. **107**(24): p. 10914-9.
36. Miller, L.W., et al., *In vivo protein labeling with trimethoprim conjugates: a flexible chemical tag.* Nat Methods, 2005. **2**(4): p. 255-7.
37. Rajapakse, H.E., et al., *Time-resolved luminescence resonance energy transfer imaging of protein-protein interactions in living cells.* Proc Natl Acad Sci U S A, 2010. **107**(31): p. 13582-7.
38. Rajapakse, H.E., et al., *Luminescent terbium protein labels for time-resolved microscopy and screening.* Angew Chem Int Ed Engl, 2009. **48**(27): p. 4990-2.
39. Seveus, L., et al., *Time-resolved fluorescence imaging of europium chelate label in immunohistochemistry and in situ hybridization.* Cytometry, 1992. **13**(4): p. 329-38.
40. Blomberg, K.R., et al., *A dissociative fluorescence enhancement technique for one-step time-resolved immunoassays.* Anal Bioanal Chem, 2011. **399**(4): p. 1677-82.
41. Lavis, L.D. and R.T. Raines, *Bright ideas for chemical biology.* ACS Chem Biol, 2008. **3**(3): p. 142-55.
42. Resch-Genger, U., et al., *Quantum dots versus organic dyes as fluorescent labels.* Nat Methods, 2008. **5**(9): p. 763-75.
43. Alivisatos, A.P., W. Gu, and C. Larabell, *Quantum dots as cellular probes.* Annu Rev Biomed Eng, 2005. **7**: p. 55-76.
44. Zhang, X., et al., *Efficient functionalization of aqueous CdSe/ZnS nanocrystals using small-molecule chemical activators.* Chem Commun (Camb), 2011. **47**(12): p. 3532-4.

45. Eliseeva, S.V. and J.C. Bunzli, *Lanthanide luminescence for functional materials and bio-sciences.* Chem Soc Rev, 2010. **39**(1): p. 189-227.
46. Selvin, P.R. and J.E. Hearst, *Luminescence energy transfer using a terbium chelate: improvements on fluorescence energy transfer.* Proc Natl Acad Sci U S A, 1994. **91**(21): p. 10024-8.
47. Selvin, P.R., *Fluorescence resonance energy transfer.* Methods Enzymol, 1995. **246**: p. 300-34.
48. Selvin, P.R., *Principles and biophysical applications of lanthanide-based probes.* Annu Rev Biophys Biomol Struct, 2002. **31**: p. 275-302.
49. Hanaoka, K., et al., *Time-resolved long-lived luminescence imaging method employing luminescent lanthanide probes with a new microscopy system.* J Am Chem Soc, 2007. **129**(44): p. 13502-9.
50. Song, B., et al., *Time-resolved luminescence microscopy of bimetallic lanthanide helicates in living cells.* Org Biomol Chem, 2008. **6**(22): p. 4125-33.
51. Zhang, Y. and L.C. Yu, *Single-cell microinjection technology in cell biology.* Bioessays, 2008. **30**(6): p. 606-10.
52. Heitz, F., M.C. Morris, and G. Divita, *Twenty years of cell-penetrating peptides: from molecular mechanisms to therapeutics.* Br J Pharmacol, 2009. **157**(2): p. 195-206.
53. Laughlin, S.T. and C.R. Bertozzi, *Imaging the glycome.* Proc Natl Acad Sci U S A, 2009. **106**(1): p. 12-7.
54. Gupta, B., T.S. Levchenko, and V.P. Torchilin, *Intracellular delivery of large molecules and small particles by cell-penetrating proteins and peptides.* Adv Drug Deliv Rev, 2005. **57**(4): p. 637-51.
55. Zhao, X., et al., *Active scaffolds for on-demand drug and cell delivery.* Proc Natl Acad Sci U S A, 2011. **108**(1): p. 67-72.
56. Hyman, J.M., et al., *A molecular method for the delivery of small molecules and proteins across the cell wall of algae using molecular transporters.* Proc Natl Acad Sci U S A, 2012. **109**(33): p. 13225-30.
57. Graessmann, M. and A. Graessmann, *Microinjection of tissue culture cells.* Methods Enzymol, 1983. **101**: p. 482-92.
58. Bao, G., W.J. Rhee, and A. Tsourkas, *Fluorescent probes for live-cell RNA detection.* Annu Rev Biomed Eng, 2009. **11**: p. 25-47.
59. Walev, I., et al., *Delivery of proteins into living cells by reversible membrane permeabilization with streptolysin-O.* Proc Natl Acad Sci U S A, 2001. **98**(6): p. 3185-90.
60. Miyamoto, K., et al., *Reversible membrane permeabilization of mammalian cells treated with digitonin and its use for inducing nuclear reprogramming by Xenopus egg extracts.* Cloning Stem Cells, 2008. **10**(4): p. 535-42.
61. Okada, C.Y. and M. Rechsteiner, *Introduction of macromolecules into cultured mammalian cells by osmotic lysis of pinocytic vesicles.* Cell, 1982. **29**(1): p. 33-41.
62. Derossi, D., et al., *The third helix of the Antennapedia homeodomain translocates through biological membranes.* J Biol Chem, 1994. **269**(14): p. 10444-50.
63. Morris, M.C., et al., *Cell-penetrating peptides: from molecular mechanisms to therapeutics.* Biol Cell, 2008. **100**(4): p. 201-17.
64. Wender, P.A., et al., *The design, synthesis, and evaluation of molecules that enable or enhance cellular uptake: peptoid molecular transporters.* Proc Natl Acad Sci U S A, 2000. **97**(24): p. 13003-8.

65. Frankel, A.D. and C.O. Pabo, *Cellular uptake of the tat protein from human immunodeficiency virus.* Cell, 1988. **55**(6): p. 1189-93.
66. Green, M. and P.M. Loewenstein, *Autonomous functional domains of chemically synthesized human immunodeficiency virus tat trans-activator protein.* Cell, 1988. **55**(6): p. 1179-88.
67. Joliot, A., et al., *Antennapedia homeobox peptide regulates neural morphogenesis.* Proc Natl Acad Sci U S A, 1991. **88**(5): p. 1864-8.
68. Schwarze, S.R., et al., *In vivo protein transduction: delivery of a biologically active protein into the mouse.* Science, 1999. **285**(5433): p. 1569-72.
69. Schwarze, S.R. and S.F. Dowdy, *In vivo protein transduction: intracellular delivery of biologically active proteins, compounds and DNA.* Trends Pharmacol Sci, 2000. **21**(2): p. 45-8.
70. Schwarze, S.R., K.A. Hruska, and S.F. Dowdy, *Protein transduction: unrestricted delivery into all cells?* Trends Cell Biol, 2000. **10**(7): p. 290-5.
71. Lindgren, M., et al., *Cell-penetrating peptides.* Trends Pharmacol Sci, 2000. **21**(3): p. 99-103.
72. Jarver, P. and U. Langel, *The use of cell-penetrating peptides as a tool for gene regulation.* Drug Discov Today, 2004. **9**(9): p. 395-402.
73. Joliot, A. and A. Prochiantz, *Transduction peptides: from technology to physiology.* Nat Cell Biol, 2004. **6**(3): p. 189-96.
74. Snyder, E.L. and S.F. Dowdy, *Recent advances in the use of protein transduction domains for the delivery of peptides, proteins and nucleic acids in vivo.* Expert Opin Drug Deliv, 2005. **2**(1): p. 43-51.
75. Futaki, S., et al., *Arginine-rich peptides. An abundant source of membrane-permeable peptides having potential as carriers for intracellular protein delivery.* J Biol Chem, 2001. **276**(8): p. 5836-40.
76. Futaki, S., *Arginine-rich peptides: potential for intracellular delivery of macromolecules and the mystery of the translocation mechanisms.* Int J Pharm, 2002. **245**(1-2): p. 1-7.
77. Luedtke, N.W., P. Carmichael, and Y. Tor, *Cellular uptake of aminoglycosides, guanidinoglycosides, and poly-arginine.* J Am Chem Soc, 2003. **125**(41): p. 12374-5.
78. Futaki, S., *Oligoarginine vectors for intracellular delivery: design and cellular-uptake mechanisms.* Biopolymers, 2006. **84**(3): p. 241-9.
79. Fretz, M.M., et al., *Temperature-, concentration- and cholesterol-dependent translocation of L- and D-octa-arginine across the plasma and nuclear membrane of CD34+ leukaemia cells.* Biochem J, 2007. **403**(2): p. 335-42.
80. Futaki, S., et al., *Arginine-rich peptides and their internalization mechanisms.* Biochem Soc Trans, 2007. **35**(Pt 4): p. 784-7.
81. Koren, E. and V.P. Torchilin, *Cell-penetrating peptides: breaking through to the other side.* Trends Mol Med, 2012. **18**(7): p. 385-93.
82. Shi Kam, N.W., et al., *Nanotube molecular transporters: internalization of carbon nanotube-protein conjugates into Mammalian cells.* J Am Chem Soc, 2004. **126**(22): p. 6850-1.
83. Su, Y., et al., *Membrane-bound dynamic structure of an arginine-rich cell-penetrating peptide, the protein transduction domain of HIV TAT, from solid-state NMR.* Biochemistry, 2010. **49**(29): p. 6009-20.

84. Madani, F., et al., *Mechanisms of cellular uptake of cell-penetrating peptides.* J Biophys, 2011. **2011**: p. 414729.
85. Zorko, M. and U. Langel, *Cell-penetrating peptides: mechanism and kinetics of cargo delivery.* Adv Drug Deliv Rev, 2005. **57**(4): p. 529-45.
86. Torchilin, V.P., *Cell penetrating peptide-modified pharmaceutical nanocarriers for intracellular drug and gene delivery.* Biopolymers, 2008. **90**(5): p. 604-10.
87. Conner, S.D. and S.L. Schmid, *Regulated portals of entry into the cell.* Nature, 2003. **422**(6927): p. 37-44.
88. Mayor, S. and R.E. Pagano, *Pathways of clathrin-independent endocytosis.* Nat Rev Mol Cell Biol, 2007. **8**(8): p. 603-12.
89. Mukherjee, S., R.N. Ghosh, and F.R. Maxfield, *Endocytosis.* Physiol Rev, 1997. **77**(3): p. 759-803.
90. Wadia, J.S., R.V. Stan, and S.F. Dowdy, *Transducible TAT-HA fusogenic peptide enhances escape of TAT-fusion proteins after lipid raft macropinocytosis.* Nat Med, 2004. **10**(3): p. 310-5.
91. Duchardt, F., et al., *A comprehensive model for the cellular uptake of cationic cell-penetrating peptides.* Traffic, 2007. **8**(7): p. 848-66.
92. Torchilin, V.P., et al., *TAT peptide on the surface of liposomes affords their efficient intracellular delivery even at low temperature and in the presence of metabolic inhibitors.* Proc Natl Acad Sci U S A, 2001. **98**(15): p. 8786-91.
93. Wunderbaldinger, P., L. Josephson, and R. Weissleder, *Tat peptide directs enhanced clearance and hepatic permeability of magnetic nanoparticles.* Bioconjug Chem, 2002. **13**(2): p. 264-8.
94. Tunnemann, G., et al., *Cargo-dependent mode of uptake and bioavailability of TAT-containing proteins and peptides in living cells.* FASEB J, 2006. **20**(11): p. 1775-84.
95. Herce, H.D. and A.E. Garcia, *Cell penetrating peptides: how do they do it?* J Biol Phys, 2007. **33**(5-6): p. 345-56.
96. Ziegler, A. and J. Seelig, *Interaction of the protein transduction domain of HIV-1 TAT with heparan sulfate: binding mechanism and thermodynamic parameters.* Biophys J, 2004. **86**(1 Pt 1): p. 254-63.
97. Richard, J.P., et al., *Cell-penetrating peptides. A reevaluation of the mechanism of cellular uptake.* J Biol Chem, 2003. **278**(1): p. 585-90.
98. Montgomery, C.P., et al., *Cell-penetrating metal complex optical probes: targeted and responsive systems based on lanthanide luminescence.* Acc Chem Res, 2009. **42**(7): p. 925-37.
99. Jaffe, L.A. and M. Terasaki, *Quantitative microinjection of oocytes, eggs, and embryos.* Methods Cell Biol, 2004. **74**: p. 219-42.
100. McNeil, P.L. and E. Warder, *Glass beads load macromolecules into living cells.* J Cell Sci, 1987. **88 (Pt 5)**: p. 669-78.
101. Gahlaut, N. and L.W. Miller, *Time-resolved microscopy for imaging lanthanide luminescence in living cells.* Cytometry A, 2010. **77**(12): p. 1113-25.
102. Ahnert-Hilger, G., et al., *Introduction of macromolecules into bovine adrenal medullary chromaffin cells and rat pheochromocytoma cells (PC12) by permeabilization with streptolysin O: inhibitory effect of tetanus toxin on catecholamine secretion.* J Neurochem, 1989. **52**(6): p. 1751-8.

103. Lee, G.M., *Measurement of volume injected into individual cells by quantitative fluorescence microscopy.* J Cell Sci, 1989. **94 (Pt 3)**: p. 443-7.
104. Sala, F. and A. Hernandez-Cruz, *Calcium diffusion modeling in a spherical neuron. Relevance of buffering properties.* Biophys J, 1990. **57**(2): p. 313-24.
105. Niswender, K.D., et al., *Quantitative imaging of green fluorescent protein in cultured cells: comparison of microscopic techniques, use in fusion proteins and detection limits.* J Microsc, 1995. **180**(Pt 2): p. 109-16.
106. Marks, K.M. and G.P. Nolan, *Chemical labeling strategies for cell biology.* Nat Methods, 2006. **3**(8): p. 591-6.
107. Carreon, J.R., et al., *Cyanine dye conjugates as probes for live cell imaging.* Bioorg Med Chem Lett, 2007. **17**(18): p. 5182-5.
108. Jones, S.A., et al., *Fast, three-dimensional super-resolution imaging of live cells.* Nat Methods, 2011. **8**(6): p. 499-508.
109. Bunzli, J.C., *Lanthanide luminescence for biomedical analyses and imaging.* Chem Rev, 2010. **110**(5): p. 2729-55.
110. Reddy, D.R., L.E. Pedro Rosa, and L.W. Miller, *Luminescent trimethoprim-polyaminocarboxylate lanthanide complex conjugates for selective protein labeling and time-resolved bioassays.* Bioconjug Chem, 2011. **22**(7): p. 1402-9.
111. Mohandessi, S., et al., *Cell-penetrating peptides as delivery vehicles for a protein-targeted terbium complex.* Chemistry, 2012. **18**(35): p. 10825-9.
112. Shaner, N.C., et al., *Improving the photostability of bright monomeric orange and red fluorescent proteins.* Nat Methods, 2008. **5**(6): p. 545-51.
113. Xu, J., et al., *Octadentate cages of Tb(III) 2-hydroxyisophthalamides: a new standard for luminescent lanthanide labels.* J Am Chem Soc, 2011. **133**(49): p. 19900-10.
114. Kosuge, M., et al., *Cellular internalization and distribution of arginine-rich peptides as a function of extracellular peptide concentration, serum, and plasma membrane associated proteoglycans.* Bioconjug Chem, 2008. **19**(3): p. 656-64.
115. Trehin, R., et al., *Metabolic cleavage of cell-penetrating peptides in contact with epithelial models: human calcitonin (hCT)-derived peptides, Tat(47-57) and penetratin(43-58).* Biochem J, 2004. **382**(Pt 3): p. 945-56.
116. Ter-Avetisyan, G., et al., *Cell entry of arginine-rich peptides is independent of endocytosis.* J Biol Chem, 2009. **284**(6): p. 3370-8.
117. Bhorade, R., et al., *Macrocyclic chelators with paramagnetic cations are internalized into mammalian cells via a HIV-tat derived membrane translocation peptide.* Bioconjug Chem, 2000. **11**(3): p. 301-5.
118. Endres, P.J., et al., *Cell-permeable MR contrast agents with increased intracellular retention.* Bioconjug Chem, 2008. **19**(10): p. 2049-59.
119. Major, J.L. and T.J. Meade, *Bioresponsive, cell-penetrating, and multimeric MR contrast agents.* Acc Chem Res, 2009. **42**(7): p. 893-903.
120. Los, G.V., et al., *HaloTag: a novel protein labeling technology for cell imaging and protein analysis.* ACS Chem Biol, 2008. **3**(6): p. 373-82.
121. Gautier, A., et al., *An engineered protein tag for multiprotein labeling in living cells.* Chemistry & Biology, 2008. **15**(2): p. 128-136.
122. Rothbard, J.B., et al., *Role of membrane potential and hydrogen bonding in the mechanism of translocation of guanidinium-rich peptides into cells.* Journal of the American Chemical Society, 2004. **126**(31): p. 9506-9507.

123. Mishra, A., et al., *HIV TAT forms pores in membranes by inducing saddle-splay curvature: potential role of bidentate hydrogen bonding.* Angew Chem Int Ed Engl, 2008. **47**(16): p. 2986-9.
124. Verdurmen, W.P., et al., *Cationic cell-penetrating peptides induce ceramide formation via acid sphingomyelinase: implications for uptake.* J Control Release, 2010. **147**(2): p. 171-9.
125. Ha, T. and P. Tinnefeld, *Photophysics of fluorescent probes for single-molecule biophysics and super-resolution imaging.* Annu Rev Phys Chem, 2012. **63**: p. 595-617.
126. Lee, H.L., et al., *Single-molecule motions of oligoarginine transporter conjugates on the plasma membrane of Chinese hamster ovary cells.* J Am Chem Soc, 2008. **130**(29): p. 9364-70.
127. Barnett, E.M., et al., *Single-cell imaging of retinal ganglion cell apoptosis with a cell-penetrating, activatable peptide probe in an in vivo glaucoma model.* Proc Natl Acad Sci U S A, 2009. **106**(23): p. 9391-6.

VITA

NAME: Shabnam Mohandessi

EDUCATION: B.Sc. Chemistry, Shahid Beheshti University (BSU), Tehran, Iran, 2003

M.Sc. Organic Chemistry, Chemistry&Chemical Engineering Research Center of Iran, Tehran,Iran, 2006**,**

PhD. , Biochemistry, University of Illinois at Chicago (UIC), Chicago, IL, 2013

TEACHING: CHEM 101, General Chemistry**;** CHEM 114, Physical Chemistry**;** CHEM 452, General Biochemistry; CHEM 455, General Biochemistry laboratory.

HONORS:

1. Center for the Physics of Living Cells (CPLC) Summer School, a practicum in single molecule imaging, supervisor: Professor Ha, University of Illinois at Urbana- Champaign (May 2012)
2. Student Presenter's travel award (May2012).
3. LAS PhD Student Award (May 2012).
4. Journal reviewer for Molecular Biosystems articles, RSC Publishing (September 2011& May 2012).
5. UIC Graduate Student Council (GSC) Travel Award (April 2012)
6. Biochemistry Representative, University of Illinois at Chicago (UIC) (May 2011)
7. American Chemical Society
8. Royal Society of Chemistry
9. Gordon Research Conferences (GRC) &Gordon Research Seminar (GRS), **2012**, Ventura, CA, USA.
10. 4^{TH} Annual Chicago Organic Symposium, University of Illinois at Chicago (UIC), **2012**, Chicago, IL, USA.
11. 2012 Student Research Forum in University of Illinois at Chicago (UIC), **2012**, Chicago, IL, USA.
12. 3^{rd} Annual SES Poster Session in Department of Chemistry at University of Illinois at Chicago (UIC)**, 2012**, Chicago, IL, USA.

PUBLICATION:

1. Vaasa, Angela; Ligi, Kadri; **Mohandessi, Shabnam**; Enkvist, Erki; Uri, Asko; Miller, Lawrence W. Time-gated luminescence microscopy with responsive nonmetal probes for mapping activity of protein kinases in living cells, Chemical Communications **2012**, 48, 8595.
2. **Mohandessi, Shabnam**; Rajendran, Megha; Magda, Darren; Miller, Lawrence W. Cell- penetrating peptides as delivery vehicles for lanthanide protein labels, Chemistry- A European Journal **2012**,18, 35, 10825.
3. Darabi, Hossein Reza; **Mohandessi, Shabnam**; Balavar, Yadollah; Moghaddam, Mojtaba Mirhosseini; Aghapoor, Kioumars; Mohsenzadeh, Farshid; Nourinia, Abbas Ali. Clove bud oil: efficient, economical and widely available oil for the inhibition of wheat seed germination, Environmental Chemistry Letters **2011**, 9, 4, 519.
4. Zhang, Xi; **Mohandessi, Shabnam**; Miller, Lawrence W.; Snee, Preston T. Efficient functionalization of aqueous CdSe/ZnS nanocrystals using small-molecule chemical activators, Chemical Communications **2011**, 47, 12, 3532.
5. Rajapakse, Harsha E.; Gahlaut, Nivriti; **Mohandessi, Shabnam**; Mohandessi, Shabnam; Yu, D; Turner, Jerrold R. Time-resolved luminescence resonance energy transfer imaging of protein-protein interactions in living cells, Proceedings of the National Academy of Sciences of the United States of America (PNAS) **2010**, 107, 31,13582.
6. Rajapakse,Harsha E.;Reddy, D. Rajasekhar; **Mohandessi, Shabnam**; Butlin, Nathaniel G.; Miller, Lawrence W.. Luminescent Terbium Protein Labels for Time-Resolved Microscopy and Screening, Angewandte Chemie- International **2009**, 48, 27, 4990.
7. Darabi, Hossein Reza; **Mohandessi, Shabnam**; Aghapoor, Kioumars; Mohsenzadeh, Farshid; Karouei, Mohammad Hashemi; Tahoori, Fatemeh; Herges, Rainer. Thioamidation of Single-Walled Carbon Nanotubes: a New Chemical Functionalization Protocol by the Willgerodt-Kindler Reaction, Australian Journal of Chemsitry **2009**, 62, 5, 413.
8. Darabi, Hossein Reza; **Mohandessi, Shabnam**; Balavar, Yadollah; Aghapoor, Kioumars. A structure-activity relationship study on a natural germination inhibitor, 2-methoxy-4-vinylphenol (MVP), in wheat seeds to evaluate its mode of action, Zeitschifift Fur Naturforschung Section C-A Journal of Biosceinces **2007**, 62, 9-10, 694.
9. Darabi, Hossein Reza; **Mohandessi, Shabnam**; Aghapoor, Kioumars; Mohsenzadeh, Farshid. A recyclable and highly effective sulfamic acid/MeOH catalytic system for the synthesis of quinoxalines at room temperature, Catalysis Communications **2007**, 8, 3, 389.